Dynamics of an impact oscillator near a degenerate graze

D R J Chillingworth

School of Mathematics, University of Southampton, Southampton SO17 1BJ, UK

E-mail: `drjc@maths.soton.ac.uk`

Abstract. We give a complete analysis of low-velocity dynamics close to grazing for a generic one degree of freedom impact oscillator. This includes nondegenerate (quadratic) grazing and minimally degenerate (cubic) grazing, corresponding respectively to nondegenerate and degenerate *chatter*. We also describe the dynamics associated with generic one-parameter bifurcation at a more degenerate (quartic) graze, showing in particular how this gives rise to the often-observed highly convoluted structure in the stable manifolds of chattering orbits. The approach adopted is geometric, using methods from singularity theory.

AMS classification scheme numbers: 34A36,34C23,37B55,70K40,70K50,70G60

1. Introduction

The theory of forced nonlinear oscillations has well known and widespread applications in science and engineering: see Hayashi [24], Fidlin [20], for example, as well as landmark texts Andronov *et al.* [2], Schmidt *et al.* [37], Guckenheimer *et al.* [23]. However, there are many engineering contexts in which oscillations are a highly undesirable feature of performance, especially when these lead to impacts between moving parts or against rigid supports, generating noise and wear and ultimately leading to mechanical breakdown: for some examples see Alzate *et al.* [1], Mason *et al.* [31], Stewart [40], Pavlovskaia *et al.* [35] as well as those described in books such as Babitsky *et al.* [5], Brogliato [8] and di Bernardo *et al.* [7].

A simple model for such dynamical impact phenomena (often called *vibro-impact* systems) is the one degree of freedom *impact oscillator*. This consists of a forced nonlinear oscillator

$$\ddot{x} + f(x, \dot{x}) = g(t) \tag{1}$$

for $x \in \mathbf{R}$, together with a *constraint* $x \geq c$ where c is a constant often called the *clearance*. Here f and g are smooth‡ functions, and as usual the dot denotes d/dt.

The model must include a prescription for how the dynamics are to proceed when $x = c$. This will typically be given by a *restitution rule* that whenever $(x, \dot{x}) = (c, v)$ then the velocity v is instantaneously replaced by $\tilde{v}$ (a function of v and perhaps other variables) satisfying $\tilde{v}v < 0$. The simplest practical example is a linear rule with $\tilde{v} = -rv$ where $0 \leq r \leq 1$, which includes the cases of perfect adherence ($r = 0$) and perfectly elastic restitution ($r = 1$). There are many variations on this model, involving more than one degree of freedom and/or more than one constraint or a non-instantaneous restitution rule. In this paper we shall require only that the linearisation of $\tilde{v}$ at $v = 0$ takes the form $-rv$ with $0 < r < 1$; thus we exclude the extreme cases.

The fact that a simple impact system can give rise to extremely complicated dynamics has long been noted, and there are many analytical and numerical studies showing complicated periodicities or convoluted orbit structures in phase space: see for example Thompson *et al.* [44], Shaw *et al.* [38], Hindmarsh *et al.* [25], Peterka *et al.* [36], Kleczka *et al.* [30], Virgin *et al.* [46], Wagg *et al.* [47],[48], Valente *et al.* [45]. Nevertheless, even a 1-degree of freedom linear oscillator with a linear restitution rule is still poorly understood from the overall dynamical point of view.

A more systematic attack on the global problem was undertaken by Whiston in a pioneering series of papers [49],[50],[51]; this enterprise inspired much subsequent work including Budd *et al.* [15], Lamba [28], Nordmark [33] as well as the present paper.

A key feature of impact oscillator dynamics that gives it a different flavour from (smooth) nonlinear dynamics is the phenomenon of *grazing* where a periodic orbit reaches the obstacle with zero velocity and nonzero acceleration: small perturbations of such orbits may or may not exhibit impacts. The resulting bifurcation phenomena have been studied by many authors including Budd *et al.* [14], Chin *et al.* [17], Dankowitz *et al.* [18], Foale *et al.* [21], Ivanov [29], Nordmark [33],[34], Szalai *et al.* [42], Molenaar *et al.* [32], Zhao *et al.* [53].

Another important aspect of impact oscillator dynamics that attracts particular interest is the low-velocity behaviour close to impact, characterised by the phenomenon of *chatter*. On leaving $x = c$ with small positive velocity but negative acceleration the orbit (i.e. the solution to (1)) may return to hit $x = c$ again after a short time; after restitution at the impact the process will repeat, and under suitable conditions the orbit may come to rest at $x = c$ after a finite time but an infinite number of such impacts. It will remain stuck at the obstacle $x = c$ until such time as the acceleration (from the forcing) becomes positive and it once again lifts off into the region $x > c$. See for example Demeio *et al.* [19] for a simple mechanical realisation of this phenomenon, or Stone *et al.* [41], Valente *et al.* [45] for more complicated dynamical settings. The first systematic

‡ For simplicity we take *smooth* to mean C^∞, although many of the results will clearly hold with less differentiability.

analytic and geometrical analysis of the dynamics of chatter was carried out by Budd *et al.* [14], using a combination of insightful numerics supported theoretically by first and second order approximations. In this paper we extend those results by providing a complete and rigorous analysis of chatter for generic impact oscillator systems (1) and for generic 1-parameter families of such systems.

In many applications the function g in (1) is periodic with period $T > 0$. In this case a standard technique for studying a forced oscillator such as (1) without the impacts is to focus on the the discrete dynamical system F that samples the solutions at times $\{nT : n \in \mathbf{Z}\}$: then periodic solutions of (1) correspond to periodic orbits of F, and so on. When impacts are introduced, however, this is no longer appropriate since the influence of the obstacle on a given trajectory cannot be expected to be T-periodic. A common approach to dealing with this problem, used by Shaw *et al.* [38], Thompson *et al.* [44], Whiston [50] and others, is first to regard (1) as an autonomous system in $\mathbf{R}^3$ by including the equation $\dot{t} = 1$ and then to consider the plane $x = c$ and the discrete dynamical system defined on it by the *first return* of trajectories after impacting the obstacle. This fits naturally with the geometry of the physical description of (1), but the resulting discrete system now has loci of discontinuity that arise from grazing trajectories. It is not easy in this setting to see how the discontinuities and the associated dynamical phenomena respond to change in initial conditions and/or governing parameters such as the clearance.

In this paper we use an alternative geometric approach, first set out in [16], which allows greater insight into the geometry of discontinuities and their influence on dynamics by replacing the picture of curved orbits intersecting a flat obstacle with an equivalent picture of straightened-out orbits intersecting a curved obstacle: the *impact surface*. See Section 2 below for the precise description. From this point of view, the problem of analysing the geometry of orbits at and near grazing becomes more readily amenable to the tools of local differential topology, dynamical systems and singularity theory.

Taking this approach, we look again at the phenomena of *grazing* and *chatter* in the light of the geometry of the impact surface. We first use this to provide rigorous underpinning for the key results in [14] that are based on approximations: by placing the results in a wider context we are able to give a full analysis of the local dynamical phenomena. We then extend this to cover the case of the discontinuous bifurcations that arise in the neighbourhood of a doubly-degenerate graze as the clearance or some other parameter is varied and the degeneracy is unfolded. In particular we exhibit the key mechanism for the creation of multiple-loop structures in stable manifolds of chatter points, which is a first step in understanding the multiple-loop patterns observed numerically for attractors and basins of attraction of periodic orbits in impact oscillators: see [50, Figure 17], [14, Figures 4 and 19], as well as [6, Figure 3] and [7] (in particular the front cover). Taken together, the results of the present paper provide a complete description of generic low-velocity impact dynamics and 1-parameter bifurcations.

2. Geometrical model for dynamics: the impact surface

We begin by recalling the construction described in Chillingworth [16] for modelling the overall dynamics of a one degree of freedom impact oscillator. The model is based on a 2-dimensional surface in three dimensions that characterises the impacts, together with certain natural maps associated with it that represent the dynamics. A similar geometrical construction was used by Sotomayor *et al.* [39], albeit with a different dynamical interpretation, to classify local vector fields on a manifold with boundary.

2.1. The impact surface and associated maps

Let $x(b, v, \tau; t)$ denote the unique solution to (1) with initial data

$$(x, \dot{x}) = (b, v) \quad \text{when} \quad t = \tau.$$

For fixed choice of $c \in \mathbf{R}$ we then write

$$x_c(\tau, v; t) := x(c, v, \tau; \tau + t)$$

so that

$$x_c(\tau, v; 0) = c, \quad \dot{x}_c(\tau, v; 0) = v. \tag{2}$$

Definition 2.1 *The* impact surface V_c *is the locus of points among all the solutions where impact occurs, that is*

$$V_c := \{(\tau, v; t) \in \mathbf{R}^3 : x_c(\tau, v; t) = c\}.$$

Note that in [16] the convention was to write $(v, \tau; t)$ rather than $(\tau, v; t)$: we trust no confusion will arise from this notation reversal.

By definition V_c contains the plane $t = 0$, which we shall denote by Π and which plays a key role in our formulation of the dynamics. It is proved in [16, Lemma 1] that V_c is indeed a surface (smooth 2-manifold), with the exception of the points on the τ-axis Π_0 and possibly certain other points where $v = 0$, characterised precisely in terms of the functions f and g in (1) and the clearance c. It is shown§ in [16, Proposition 1] (see also [14] where it is inherent in the analysis, and see the calculations below) that in a neighbourhood of Π_0 the impact surface V_c consists of two sheets (smooth 2-manifolds) intersecting transversely along Π_0. One of these is of course the plane Π while the other sheet V_c' is represented in a neighbourhood of Π_0 as the graph of a smooth function $v = v_c(\tau, t)$ given implicitly by

$$y_c(\tau, v_c; t) = 0 \tag{3}$$

when x_c is written in the form

$$x_c = c + t y_c(\tau, v; t) \tag{4}$$

§ The statement $r \geq 2$ there is an error: it originally referred to degree of differentiability, and has no connection with the restitution coefficient here.

for a smooth function y_c on a neighbourhood of Π_0 in $\mathbf{R}^3$.

By implicit differentiation of (3) we find

$$\frac{\partial}{\partial t}\, v_c(\tau, t)|_{t=0} = -\tfrac{1}{2}a_c(\tau) \tag{5}$$

where $a_c(\tau) := \ddot{x}_c(\tau, 0; 0)$ is the initial acceleration (again see [14] as well as [16, Proposition 1]).

There are three maps which we use to build the dynamical model for the impact oscillator. We now describe each of these in turn.

2.1.1. The projection p_c. Consider the projection

$$p : \mathbf{R}^3 \to \Pi : (\tau, v; t) \mapsto (\tau, v)$$

from $\mathbf{R}^3$ to the plane Π of initial data, and let p_c denote its restriction to V_c':

$$p_c := p|V_c' : V_c' \to \Pi.$$

Let H_c be the set of singular points of $p_c : V_c' \to \Pi$ (including those, if any, where V_c' itself may be singular). From the Implicit Function Theorem it is immediate that

$$H_c = \{(\tau, v; t) \in V_c' : \dot{x}_c(\tau, v; t) = 0\}$$

which in geometric terms is the *horizon* of V_c' as viewed along the t-direction. Dynamically, the points of H_c represent *graze* points, that is points where the solution to (1) meets the obstacle $x = c$ with zero velocity. See Figure 1, where for diagrammatic simplicity the curve H_c is not distinguished from the horizon of V_c' as seen from the viewpoint of the reader: in reality these are of course different. The subset $P_c := p(H_c)$ of Π is the *apparent outline* (classically the *apparent contour*) of the surface V_c' in the t-direction: see Bruce [10], Bruce *et al.* [12].

The generic local geometry of smooth maps from a smooth surface M into $\mathbf{R}^2$ is well understood since the work of Whitney [52]. The set of singular points is a smooth 1-manifold in M consisting of arcs of *fold points* (where the singular set maps locally to a smooth 1-manifold) and isolated *cusp points* (where the singular set maps locally to a $\frac{3}{2}$-power cusp). The precise characterisations are given in terms of partial derivatives, and local coordinates can be chosen so that at fold points or cusp points the map has the form $(x, y) \mapsto (x, y^2)$ or $(x, y) \mapsto (x, xy + y^3)$ respectively. These generic results apply also to the conceivably more restricted setting of projection of a surface in $\mathbf{R}^3$ to a plane, and thus to the geometry of apparent outlines. In Figure 1 the points w_1, w_3 are images of fold points, while w_2 is the image of a cusp point.

As the surface or the view direction varies with one or more parameters the outline will typically undergo certain local transitions. The generic 1-parameter transitions in apparent outlines are also well understood: see [3],[9],[13] and Figure 2.

In general, without any restriction on t, there may be regions of Π filled densely by arcs of P_c. However, if V_c is periodic in t (as may happen for undamped linear systems
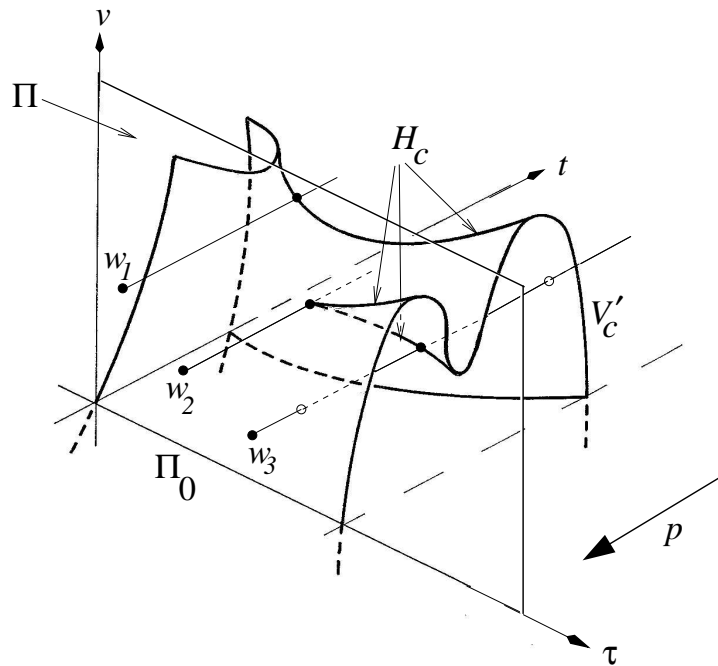
Figure 1. The impact surface $V_c = \Pi \cup V'_c$ with horizon H_c that is the set of singular points of the projection $p|V'_c \to \Pi$. Points w_1, w_2, w_3 belong to the apparent outline $P_c = p(H_c)$ (not shown).

with periodic forcing) or we restrict to a compact subset of V_c then this complication will not arise.

It is pertinent to ask whether for arbitrary choice of clearance c the apparent outline of the impact surface V'_c, which is determined by solutions of the differential equation (1), is indeed generic as just described, and whether the transitions in the apparent outline as c varies are also generic in this context. These questions may be posed both for a general system (1) and for a specific system such as the forced harmonic oscillator

$$\ddot{x} + x = \cos \omega t. \tag{6}$$

A detailed discussion of the generic geometry of V'_c and its outline for the general system (1) and for the linear system (6) can be found in [16] where these questions are answered.

2.1.2. The re-set map ϕ_c. There is a natural smooth *re-set map $\phi_c : V_c \to \Pi$* obtained simply by re-setting the clock to $t = 0$ at the moment of impact:

$$\phi_c : V_c \to \Pi : (\tau, v; t) \mapsto (\tau + t, \dot{x}_c(\tau, v; t)).$$
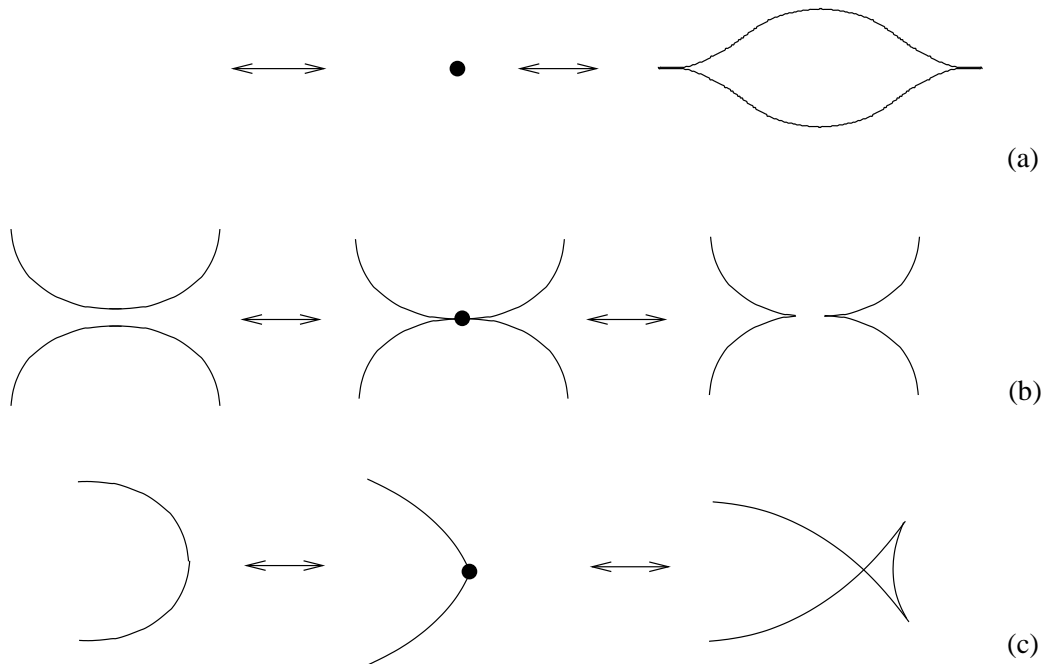
Figure 2. The three generic transitions in apparent outlines: (a) lips, (b) beaks, (c) swallowtail.

Let Z_c denote the *zero set* of V_c, that is the intersection of V_c' with the plane $v = 0$. The following facts about the singularity structure of ϕ_c are proved in [16, Propositions 6,7].

Proposition 2.2 *The singular set of ϕ_c is $Z_c \setminus \Pi_0$. Points $(\tau, 0; t) \in Z_c \setminus \Pi_0$ where $a_c(\tau) \neq 0$ are fold points of ϕ_c, while points where $a_c(\tau) = 0$ but $a_c'(\tau) \neq 0$ are cusp points.*

2.1.3. The restitution map R_c. The *restitution map* describes how the velocity immediately after impact depends on the velocity immediately before impact. Thus we write

$$\Pi^+ = \{(\tau, v) \in \Pi : v > 0\}, \qquad \Pi_0^+ = \Pi^+ \cup \Pi_0$$
$$\Pi^- = \{(\tau, v) \in \Pi : v < 0\}, \qquad \Pi_0^- = \Pi^- \cup \Pi_0$$

and we suppose that $R_c : \Pi_0^- \to \Pi_0^+$ is the restriction to Π_0^- of a map

$$R_c : \Pi \to \Pi : (\tau, v) \mapsto (\tau, \rho_c(v))$$

where $\rho_c : \mathbf{R} \to \mathbf{R}$ is a differentiable function with $\rho_c(0) = 0$ and $\rho_c'(0) < 0$. In many cases an appropriate choice is $\rho_c(v) = -rv$ with $0 < r < 1$ independent of c, although all that we shall require is that $\rho_c'(0) = -r$.

2.2. The first-hit map F_c and the dynamical system G_c

Since we are assuming the dynamics take place in the region $x \geq c$ it is only the upper half-plane Π_0^+ that is of physical interest. Nevertheless, in much of what follows it will

be useful first to consider Π as a whole and then restrict to Π_0^+ later.

The projection $p_c : V_c \to \Pi$ has a partial right inverse constructed as follows. Choose initial data $(\tau, v) \in \Pi^+$ (so $x = c$ and $\dot{x} = v > 0$ at $t = 0$), then proceed parallel to the t-axis in the direction of increasing t until the point $F_c(\tau, v)$ of first intersection (*first hit*) with V_c is reached: thus

$$F_c(\tau, v) = (\tau, v; t_1) \in V_c'$$

where $(\tau, v; t) \notin V_c$ for $0 < t < t_1$. It is possible that no such t_1 exists (no future impacts occur), but for notational simplicity we disregard such points and write

$$F_c : \Pi^+ \to V_c'$$

in any case, with the understanding that F_c may not be defined on the whole of Π^+.

The construction of F_c extends naturally to points $(\tau, 0) \in \Pi_0$ for which $x_c(\tau, 0; t) > 0$ for all sufficiently small $t > 0$; if this does not hold (for example, if $\ddot{x}_c(\tau, 0; 0) < 0$) then the constrained orbit remains stationary at $x = c$ and we define $F_c(\tau, 0) = (\tau, 0)$. The points of V_c' in the image of $F_c : \Pi_0^+ \to V_c'$ will be called *visible* points, as these are the points of V_c' that can be 'seen' from Π_0^+ along the positive t direction.

Finally, although it is not needed for dynamical purposes, for geometric convenience we define $F_c : \Pi^- \to V_c'$ analogously, proceeding here in the direction of negative t.

The first-hit map $F_c : \Pi \to V_c'$ defined in this way typically has discontinuities. Since p_c is a local diffeomorphism at points $z \in V_c' \setminus H_c$ it follows that the discontinuities of F_c must lie in the apparent outline $P_c = p(H_c)$ or on Π_0. Not all points $w \in P_c$ are discontinuity points of F_c, of course, but only those with $F_c(w) \in H_c$: thus in Figure 1 the point w_1 is a point of discontinuity of F_c while the point w_3 is not.

2.3. The correspondence principle

The task of describing the dynamics of the impact oscillator close to grazing is greatly helped by exploiting a correspondence, induced naturally by ϕ_c, between geometric features of P_c close to Π_0 and those away from Π_0.

If $z \in H_c$ then $p_c(z) \in P_c$ by definition, and since $\dot{x}_c = 0$ at z we have $\phi_c(z) \in \Pi_0$. Likewise if $z \in Z_c$ then $p_c(z) \in \Pi_0$ by definition, and it is also the case that $\phi_c(z) \in P_c$. This is because z represents current data (on $x = c$) for a solution with initial velocity $v = 0$ so, by uniqueness of solutions of (1), after re-set the point $\phi_c(z)$ represents initial data for a solution $x(t)$ with $x(t) = c$ and with $\dot{x}(t) = 0$ at some other time t. Thus

$$\phi_c(H_c) = \Pi_0 = p_c(Z_c) \quad \text{and} \quad p_c(H_c) = P_c = \phi_c(Z_c).$$

In fact by extending this argument we obtain a more general result which we leave as an exercise:

Proposition 2.3

$$p_c^{-1}(P_c \cup \Pi_0) = \phi_c^{-1}(P_c \cup \Pi_0).$$

$\square$

Furthermore, since re-setting the time clearly does not affect geometric features of the dynamics, any features of the outline P_c in a neighbourhood of $w = p_c(z) \in P_c$ where $z \in H_c$ must have counterparts in a neighbourhood of $\phi_c(z) \in \Pi_0$. This *correspondence principle* between P_c and Π_0 enables us to focus the analysis on points of Π_0 when studying local dynamics close to grazing, and (as we see below) provides a valuable framework for understanding the structure of the dynamics itself. A fuller description of the geometry associated to the correspondence principle can be found in [16].

2.4. Construction of the dynamics

We are now ready to construct the (discontinuous) discrete dynamical system on the half-plane Π_0^+ that we will use to model the dynamics of the impact oscillator.

Begin by applying the first-hit map $F_c : \Pi_0^+ \to V_c'$. This corresponds to following a solution of (1) as it leaves the obstacle at $x = c$ until it returns to $x = c$ for the first time. Next, apply the re-set map $\phi_c : V_c' \to \Pi$; this is simply a re-calibration of the time variable. Since the initial data lie in Π_0^+ the velocity at first hit must be negative or zero, so we have

$$\phi_c \circ F_c : \Pi_0^+ \to \Pi_0^-.$$

Finally apply the restitution map $R_c : \Pi_0^- \to \Pi_0^+$ and consider the composition:

$$\Pi_0^+ \xrightarrow{F_c} V_c' \xrightarrow{\phi_c} \Pi_0^- \xrightarrow{R_c} \Pi_0^+ .$$

The iteration of this process reconstructs the impact dynamics of the oscillator as a (discontinuous) discrete dynamical system on Π_0^+ generated by the map

$$G_c := R_c \circ \phi_c \circ F_c : \Pi_0^+ \to \Pi_0^+.$$

As indicated above, we may regard F_c and R_c and hence also G_c as maps defined on the whole of Π whenever this is convenient.

The rest of this paper is devoted to describing fully the generic behaviour of iterations of G_c close to the τ-axis Π_0, both for fixed clearance c and as a 1-parameter family of dynamical systems when c or another parameter is varied. We take the partial results of [14] further by giving a rigorous derivation of the dynamics for nondegenerate chatter at *regular points* of Π_0 (that is where $a_c(\tau) \neq 0$) and degenerate chatter at *tangency points* of Π_0 (where $a_c(\tau) = 0$ but the derivative $a_c'(\tau) \neq 0$). We also consider a yet more degenerate situation that generically arises only for certain values of the clearance c at so-called *swan points* of Π_0 (where $a_c(\tau) = a_c'(\tau) = 0$ but $a_c''(\tau) \neq 0$), and we show how the dynamics unfold and undergo newly-created discontinuities in a 1-parameter bifurcation as c passes through such values. The creation of new cusp

points for p_c gives rise to convoluted stable manifolds of nearby chatter points, with immediate implications for complicated global dynamical behaviour. Understanding the global structure of stable manifolds is one of the main challenges in formulating a dynamical theory for non-smooth systems such as impact oscillators.

3. Nondegenerate chatter

Let the clearance c be fixed. To simplify notation in this section we temporarily write V', F, G etc. for V'_c, F_c, G_c etc., although we retain v_c for clarity and understand that p denotes $p|V'_c$. Using coordinates (τ, v) on Π and (τ, t) on V', we identify a point $(\tau_*, 0; 0)$ of the τ–axis $\Pi_0 = \Pi \cap V'$ with both $w_* = (\tau_*, 0) \in \Pi$ and $z_* = (\tau_*, 0) \in V'$.

Let $w_* = (\tau_*, 0) \in \Pi_0$ be a *regular point* of Π_0, so that $a(\tau_*) \neq 0$. Since the 'free' dynamics take place in the region $x > c$, the behaviour of any solution that leaves $x = c$ with zero velocity but positive acceleration will not be susceptible to our local (low-velocity) analysis close to Π_0: therefore we assume $a_* := a(\tau_*) < 0$. On leaving $x = c$ with small positive velocity the solution to (1) will slow down, then possibly reverse and hit $x = c$ again after a short time. This is indeed the case as we see from (5): since $z_* \notin H$ the map $p : V' \to \Pi$ is a local diffeomorphism at z_* and therefore F is also a local diffeomorphism at w_*. From Proposition 2.2 we have that $\phi : V' \to \Pi$ is a local diffeomorphism at w_* and so $G = R \circ \phi \circ F$ is (the restriction to Π_0^+ of) a local diffeomorphism of Π at w_*.

3.1. Local linearisation along Π_0

As a first approximation to the dynamics we linearise at the equilibrium point $w_* \in \Pi_0$. Since by definition

$$G \circ p = R \circ \phi$$

we have on differentiation

$$DG(w)Dp(z) = DR(u)D\phi(z)$$

for $z \in V'$ where $w = p(z)$ and $u = \phi(z)$, both in Π. Writing $\tau = \tau_* + \sigma$ we see from (5) that the derivative $Dp(z_*)$ is

$$Dp(z_*) : (\sigma, t) \mapsto (\sigma, -\tfrac{1}{2}a_* t).$$

Also, implicit differentiation of (3) shows that $\frac{\partial v_c}{\partial t}(z_*) = \tfrac{1}{2}a_*$ so that (see [16, Lemma 2])

$$D\phi(z_*) : (\sigma, t) \mapsto (\sigma + t, \tfrac{1}{2}a_* t).$$

Hence the derivative of the local diffeomorphism $G = R \circ \phi \circ F$ at w_* is given by the 2×2 matrix

$$DG(w_*) = \begin{pmatrix} 1 & -\frac{2}{a_*} \\ 0 & r \end{pmatrix} \tag{7}$$

where $r = -\rho'(0)$ is the restitution coefficient (compare [14]).

Eigenvectors of $DG(w_*)$ are $(1,0)$ with eigenvalue 1 (since the τ-axis Π_0 is fixed) and $(2, a_*(1-r))$ with eigenvalue r. Therefore, to first order, we have the picture as illustrated in Figure 3(a) (see also [14]): orbits of the local linearisation of the discrete dynamics G approach Π_0 along directions with negative slope that tends to zero as $a_* \to 0$ or as $r \to 1$.
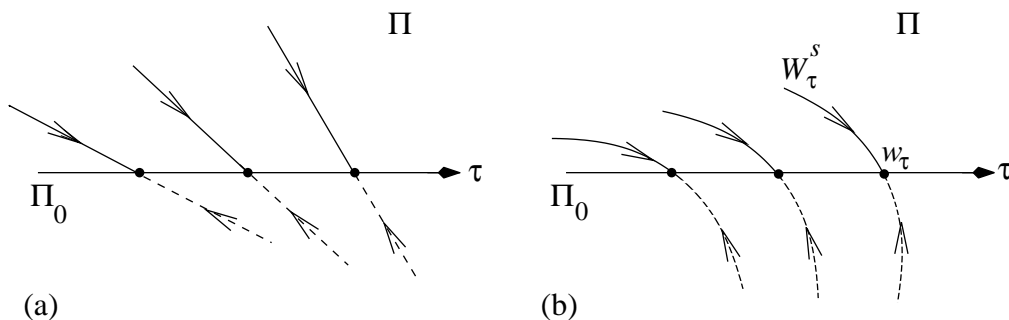
Figure 3. Local dynamics of G in the (τ, v)-plane Π close to Π_0: nondegenerate chatter for $a(\tau) < 0$. (a) Local linearisation, (b) local foliation by stable manifolds.

This does not complete the story, however, as it remains to confirm that the linear description also accurately describes the nonlinear behaviour of G on Π close to Π_0.

A fundamental component in the theory of smooth dynamical systems is the analysis of dynamics in the neighbourhood of a *normally hyperbolic* invariant manifold, that is an invariant manifold for which the rate of normal contraction or expansion overpowers any contraction or expansion along the manifold itself: main references are [26] and [43]. See also [27] for an encyclopaedic treatment.

In our case, let J be any open interval of the τ-axis Π_0 on which $a(\tau)$ is negative and bounded away from zero. Then G is the identity on J and at each point $w \in J$ the derivative $DG(w)$ has a contracting eigenspace (since $0 < r < 1$) transverse to Π_0. Hence J is a normally hyperbolic invariant manifold for G, and from the standard theory [26] we immediately deduce the following description of the local dynamics of G on some neighbourhood U of J in Π. Recall, however, that for applications to the impact oscillator we are concerned only with forward iterations of G and with the region Π_0^+, that is where $v \geq 0$.

Theorem 3.1 *For each $\tau \in J$ there is a smooth G-invariant curve W_τ^s in $U \subset \Pi$ through $w_\tau = (\tau, 0) \in \Pi_0$ and tangent to the direction $(2, (1-r)a(\tau))$. The curve W_τ^s is a local* stable manifold *for w_τ:*

$$W_\tau^s = \{u \in U : G^n(u) \to w_\tau \ as \ n \to +\infty\}.$$

The curves $\{W_\tau^s\}_{\tau \in J}$ provide a continuous foliation of U, in that there is a homeomorphism $\Phi : J \times \mathbf{R} \to U$ taking $\{\tau\} \times \mathbf{R}$ to W_τ^s for each $\tau \in J$. See Figure 3(b).

Thus the linear picture is indeed an accurate representation of the nonlinear dynamics close to Π_0, although this result yields only that the stable manifold W_τ^s varies *continuously* with τ. Can we obtain more, and see that in fact W_τ^s varies *smoothly* with τ so that the union of the W_τ^s form a *smooth foliation* of a neighbourhood of Π_0? From a result of Takens [43] the answer turns out to be positive.

Theorem 3.2 *If the functions f and g in (1) are C^∞ then (for suitable U) the homeomorphism Φ in Theorem 3.1 may be taken to be a C^∞ diffeomorphism.*

Proof. This follows from the more general (although local) theorem in [43] concerning partially hyperbolic fixed points. The *non-resonance* conditions which are imposed in the more general setting of [43] are in our case vacuously satisfied since $0 < r < 1$ and there is no expansion or contraction along the manifold J. Extension from the local result to the whole of J follows by usual compactness arguments applied to the closure of J. □

Therefore the dynamics of the local linearisation as described in [14] do indeed give an accurate picture of the true (nonlinear) dynamics up to smooth change of coordinates.

As $a(\tau) \to 0$ the stable manifold W_τ^s approaches Π_0 with slope tending to zero. Our next step is to investigate the local dynamics in this limiting case.

4. Degenerate chatter

In this section we examine the nature of chatter close to a point $w_* = (\tau_*, 0)$ where now $a_c(\tau_*) = 0$. For generic choice of the functions f and g in (1) and for an open dense set of choices of the clearance c the function $a_c(\tau)$ will have isolated zeros each with $a_c'(\tau) \neq 0$. In particular this is the case for the linear system (6), since here $a_c(\tau) = -c + \cos \omega \tau$. However, for certain values of c the function $a_c(\tau)$ can typically be expected to undergo Morse transitions (fold bifurcations) where $a_c(\tau) = 0$ and $a_c'(\tau) = 0$ while $a_c''(\tau) \neq 0$. We shall describe the local dynamics of the impact oscillator in both these situations.

We start by calculating the first few terms of the Taylor series of the maps

$$p_c : (\tau, t) \mapsto (\tau, v_c(\tau, t)) \tag{8}$$

and

$$\phi_c : (\tau, t) \mapsto (\tau + t, \dot{x}_c(\tau, v_c(\tau, t)) \tag{9}$$

at points $(\tau, 0) \in \Pi_0$. Since from (4) we have

$$v = \dot{x}_c(\tau, v; 0) = y_c(\tau, v; 0) \tag{10}$$

it follows that $\frac{\partial y_c}{\partial v} = 1$ and all other derivatives of y_c with respect to v and/or τ vanish on Π_0. Using this, by implicit differentiation of (3) and writing $\tau = \tau_* + \sigma$ we find

$$v_c(\tau_* + \sigma, t) = -\tfrac{1}{2}at \tag{11}$$

$$-\tfrac{1}{2}a'\sigma t + \tfrac{1}{2}(-\tfrac{1}{3}a' + \tfrac{1}{2}ab)t^2 \tag{12}$$

$$-\tfrac{1}{4}a''\sigma^2 t + \tfrac{1}{2}(-\tfrac{1}{3}a'' + \tfrac{1}{2}a'b)\sigma t^2 \tag{13}$$

$$-\tfrac{1}{6}(\tfrac{1}{4}a'' + \tfrac{3}{2}(-\tfrac{1}{3}a' + \tfrac{1}{2}ab)b)t^3 + O(4) \tag{14}$$

where $a = a_c(\tau_*)$, $b = \frac{\partial}{\partial v}\ddot{x}_c(\tau_*, 0; 0)$ and the primes denote derivatives with respect to τ evaluated at τ_* (which in general depend also on c). Hence, if $a \neq 0$ then

$$v_c(\tau_* + \sigma, t) = -\tfrac{1}{2}at + O(2) \tag{15}$$

while if $a = 0$ but $a' \neq 0$ then

$$v_c(\tau_* + \sigma, t) = -\tfrac{1}{6}a't(3\sigma + t) + O(3). \tag{16}$$

Finally, if $a = a' = 0$ but $a'' \neq 0$ then

$$v_c(\tau_* + \sigma, t) = -\tfrac{1}{2}4a''t(6\sigma^2 + 4\sigma t + t^2) + O(4). \tag{17}$$

4.1. Dynamics near a tangency point

A point $(\tau, 0) \in \Pi_0$ where $a_c(\tau) = 0$ and $a'_c(\tau) \neq 0$ is called a *tangency point*. In the context of Section 3 this can be regarded as a point of Π_0 where the normal hyperbolicity fails in the least degenerate way.

Suppose that $w_* = (\tau_*, 0) \in \Pi_0$ is a tangency point. From (16) we see that v_c has a saddle critical point at $(\sigma, t) = (0, 0)$. The horizon H_c is tangent to the line $3\sigma + 2t = 0$ which projects from V'_c by p_c to the graph in Π of a function

$$v = \tfrac{3}{8}a'_c(\tau_*)\sigma^2 + O(3).$$

We consider two cases separately, according to the sign of $a'_c(\tau_*)$. Again for convenience we drop the suffix c from the notation.

(a) The case $a'(\tau_*) > 0$

The points of H close to w_* have $v \geq 0$. The part of H relevant for us is the arc where $t \geq 0$, that is $\sigma \leq 0$, and so the relevant part of $P = p(H)$ here is a smooth arc P_* quadratically tangent to Π_0 at w_* from the direction $\tau < \tau_*$ and $v > 0$. This is the discontinuity set for the first-hit map F and hence for G locally: we call it the *discontinuity arc*. See Figure 4.

Theorem 4.1 *Let $w_* = (\tau_*, 0)$ be a tangency point with $a'(\tau_*) > 0$. There is a smooth arc $\gamma \subset \Pi_0^+$ with an end-point at w_*, quadratically tangent to Π_0 at w_* from the side $\tau < \tau_*$ and otherwise lying between P_* and Π_0. The arc γ is forward invariant for G (that is $G(\gamma) \subset \gamma$) and is locally unique in the sense that if γ, γ' are two such arcs then one is a subset of the other. The fixed point w_* is exponentially attracting for $G|\gamma$, while γ is weakly normally hyperbolic (repelling) for G near w_*. Orbits close to but not on γ either (if below γ) are attracted exponentially to Π_0 in nondegenerate chatter or (if above γ) cross the discontinuity arc P_* after finitely many iterations of G, corresponding to loss of immediate contact with the obstacle. See Figure 5.*

By *weakly normally hyperbolic* near w_* we mean that at points $w \in \gamma$ the derivative $DG(w)$ has an eigenvalue $\lambda \neq 1$ (in this case $\lambda > 1$) with eigendirection transverse to γ, although $\lambda \to 1$ as $w \to w_*$ along γ. The terms *above* and *below* correspond to values of v.
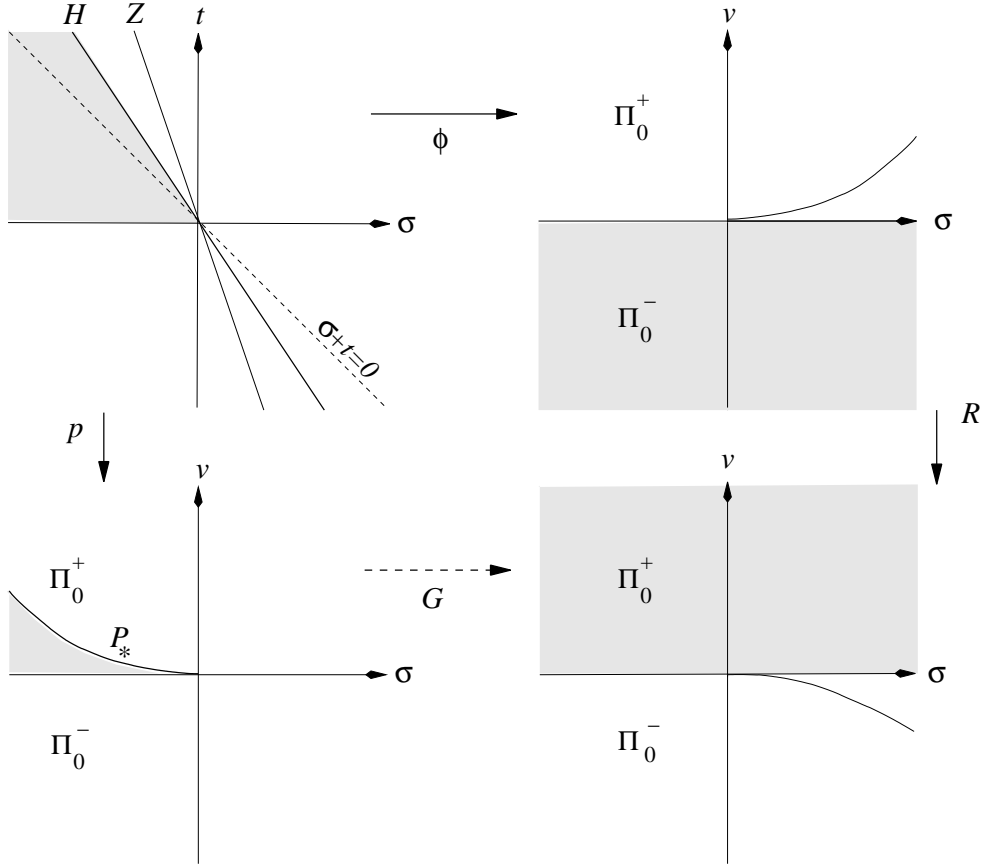
Figure 4. The actions of p, ϕ and R close to $(\tau_*, 0)$ with $a'(\tau_*) > 0$: here $\tau = \tau_* + \sigma$. The shaded area in the top left diagram represents the visible part of V', and the other shaded areas are its images under the relevant maps as indicated. The arc $P_* \subset p(H)$ is the discontinuity arc.

A proof of the existence of such an arc γ, approximately forward invariant up to second order, was given by Budd and Dux in [14]. The analysis in [14] is also for a particular linear system, although the authors observe that their results apply more generally. We provide here a complete proof that applies in full generality to nonlinear systems of type (1).

4.1.1. Proof of Theorem 4.1. From (8) and (16) we see that the projection $p_c : V' \to \Pi$ is given in local coordinates by

$$p : (\sigma, t) \mapsto (\sigma, -k(3\sigma t + t^2) + O(3)) \tag{18}$$

where $k = \frac{1}{6}a'(\tau_*) > 0$, and from (9) and (16) the reset map $\phi : V' \to \Pi$ is given by

$$\phi : (\sigma, t) \mapsto (\sigma + t, -k(3\sigma t + 2t^2) + O(3)). \tag{19}$$

Figure 4 indicates some local geometry of p and of ϕ. As already noted, to first order the horizon H is given by $3\sigma + 2t = 0$, while to first order the zero set Z is given by $3\sigma + t = 0$. Also, the line $\sigma + t = 0$ is by definition taken by ϕ to the v-axis $\sigma = 0$.
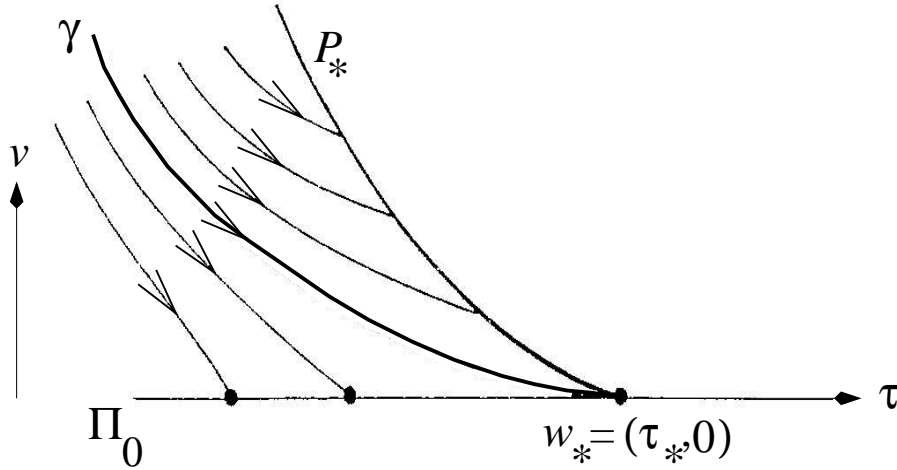
Figure 5. Degenerate chatter at $w_* = (\tau_*, 0)$ with $a'(\tau_*) > 0$. Invariant curves below the invariant curve γ represent nondegenerate chatter; invariant curves above γ carry orbits across the discontinuity arc P_*.

Now take new coordinates (σ, η) in $\mathbf{R}^2$, where $\eta = \frac{3}{2}\sigma + t$. Then

$$p : (\sigma, \eta) \mapsto (\sigma, -k\eta^2 + \tfrac{9}{4}k\sigma^2 + O(3)).$$

Composing with the diffeomorphism

$$\psi : \mathbf{R}^2 \to \mathbf{R}^2 : (u, w) \mapsto (u, w - \tfrac{9}{4}ku^2)$$

we obtain

$$\psi \circ p : (\sigma, \eta) \mapsto (\sigma, -k\eta^2 + O(3))$$

which exhibits p explicitly as a *fold* map. By standard methods of singularity theory (see e.g. Arnol'd *et al.* [4], Golubitsky *et al.* [22]), after composing with local C^∞ diffeomorphisms of $\mathbf{R}^2$ in range and domain that are the identity to second order, we may in fact assume that in a neighbourhood of $(0,0)$ we have

$$\psi \circ p : (\sigma, \eta) \mapsto (\sigma, -k\eta^2) \tag{20}$$

without any higher order terms.

Let $q : V' \to \Pi$ denote the composition $R \circ \phi$. In the new (σ, η) coordinates we find

$$\psi \circ q : (\sigma, \eta) \mapsto (\eta - \tfrac{1}{2}\sigma, -rk(2\eta^2 - 3\sigma\eta) - \tfrac{9}{4}k(\eta - \tfrac{1}{2}\sigma)^2 + O(3)) \tag{21}$$

where we recall that $R(\tau, v) = (\tau, \rho(v))$ and $r = -\rho'(0)$.

To say that γ is an invariant curve for G is equivalent to saying that the curve $\beta = F(\gamma) \subset V'$ has the property that $p(\beta) = q(\beta)$, which in turn is equivalent to saying that β is an invariant curve for the map $h := p^{-1} \circ q$ whose domain and range are subsets of V'. Explicitly we have

$$h = p^{-1} \circ q : (\sigma, \eta) \mapsto (\eta - \tfrac{1}{2}\sigma, \sqrt{Q_r(\sigma, \eta) + O(3)}) \tag{22}$$

where

$$Q_r(\sigma, \eta) := r(2\eta^2 - 3\sigma\eta) + \tfrac{9}{4}(\eta - \tfrac{1}{2}\sigma)^2. \tag{23}$$

Our strategy for finding β will be to blow up the coordinates at $(\sigma, \eta) = (0, 0)$ and then exhibit β in the new coordinates as the stable manifold of a hyperbolic fixed point of G. For the blow-up construction we write

$$(\sigma, \eta) = (s, sm) =: \chi(s, m)$$

so that m is the slope of the ray from the origin on which (σ, η) lies, and s measures displacement along the ray. Then

$$h(s, sm) = ((m - \tfrac{1}{2})s, \sqrt{s^2 Q_r(1, m) + O(s^3)})$$

and so using (s, m) as coordinates this becomes

$$h' : (s, m) \mapsto (s', m')$$

where

$$s' = (m - \tfrac{1}{2})s \tag{24}$$
$$m' = (m - \tfrac{1}{2})^{-1}\sqrt{Q_r(1, m) + O(s)}. \tag{25}$$

The domain D_r of h' is the subset of $\mathbf{R}^2$ corresponding to the values of m for which $m \neq \tfrac{1}{2}$ and the expression under the square root is nonnegative, for $|s|$ sufficiently small. The following is straightforward to check.

Proposition 4.2 *The quadratic function $m \mapsto Q_r(1, m)$ has zeros at m_-, m_+ where*

$$0 < m_- < \tfrac{1}{2} < m_+ < \tfrac{3}{2}$$

and $Q_r(1, m) > 0$ for $m \in E_r := (-\infty, m_-] \cup [m_+, \infty)$. Also $m_-, m_+ \to \tfrac{1}{2}$ as $r \to 0$. $\square$

Since two distinct zeros of a quadratic function are necessarily simple zeros, the Implicit Function Theorem yields the following result.

Corollary 4.3 *For sufficiently small $\epsilon > 0$ the domain D_r of h' contains the region $D_r(\epsilon) = D_r^-(\epsilon) \cup D_r^+(\epsilon)$ where*

$$D_r^-(\epsilon) := \{(s, m) \in \mathbf{R}^2 : |s| < \epsilon, m < \delta_-(s)\}, \tag{26}$$
$$D_r^+(\epsilon) := \{(s, m) \in \mathbf{R}^2 : |s| < \epsilon, m > \delta_+(s)\} \tag{27}$$

and $\delta_\pm$ are smooth functions with $\delta_\pm(0) = m_\pm$ respectively.

We now seek a fixed point for h' on $0 \times E_r$. This occurs where

$$m = (m - \tfrac{1}{2})^{-1} \sqrt{Q_r(1, m)},$$

that is where

$$Q_r(1, m) = m^2 (m - \tfrac{1}{2})^2. \tag{28}$$

Solutions of (28) are given by $m = \frac{3}{2}$ and by the solutions of

$$2rm = (m - \tfrac{1}{2})^2 (m + \tfrac{3}{2}). \tag{29}$$

A simple sketch of the graph of the cubic function on the right hand side of (29) shows that this equation has three solutions m_1, m_2, m_3 with

$$m_1 < -\tfrac{3}{2} \quad \text{and} \quad 0 < m_2 < \tfrac{1}{2} < m_3.$$

We now investigate these four solutions of (28) and verify that only one of them is relevant here.

Solution $m = \frac{3}{2}$: in the original (σ, t) coordinates this corresponds to $t = 0$, that is the τ-axis Π_0. Clearly this is invariant under G (on one side of $(\tau_*, 0)$) but it represents equilibrium states and is not the arc γ representing chatter that we seek. In fact $m = \frac{3}{2}$ implies $r = 1$ which is the ideal case of perfect restitution in the limit as $v \to 0$.

Solution $m_1 < -\frac{3}{2}$: the image of this line is given opposite orientations by p and q, so that under the composition $q \circ p^{-1}$ the orientation of the image is reversed. Such a curve cannot be a candidate for γ. Moreover, since the gradient of the line is less than -3 it maps under p (or q) to a curve tangent to the τ-axis but with $v \le 0$, not relevant here.

Solution $0 < m_2 < \frac{1}{2}$: the image of this line is also given opposite orientations by p and q (in particular, points with $v > 0$ are taken to points with $v < 0$) so this image cannot be a candidate for γ.

Solution $m_3 > \frac{1}{2}$: here when $t > 0$ both p and q take this line into the region $v > 0$ with the same orientation, so if $\gamma = p(\beta)$ exists as an invariant curve then the tangent direction to β at the origin must correspond to this ray.
Note that m_3 increases from $\frac{1}{2}$ to $\frac{3}{2}$ as r increases from 0 to 1.

We next study local linearisation of h' at $(0, m_3)$. Using (22) and (23) we find that the Jacobian matrix for h' at a point $(0, m)$ has the form

$$Dh'(0, m) = \begin{pmatrix} m - \tfrac{1}{2} & 0 \\ * & N_r(m) \end{pmatrix}$$

with

$$N_r(m) = Q^{-\frac{1}{2}} \left(\tfrac{1}{2}(m - \tfrac{1}{2})^{-1} [r(4m - 3) + \tfrac{9}{2}(m - \tfrac{1}{2})] - Q(m - \tfrac{1}{2})^{-2} \right) \tag{30}$$

$$= r(2m + 3)(2m - 1)^{-2} Q^{-\frac{1}{2}} \tag{31}$$

where Q stands for $Q_r(1, m)$ and where $*$ denotes a term which depends on the $O(3)$ term in ϕ. In the case when m satisfies the fixed point equation (28) this further simplifies (eliminating r) to give

$$N_r(m) = \frac{(2m+3)^2}{8m^2(2m-1)}.$$

As the eigenvalues of $Dh'(0, m)$ are $\lambda = (m - \frac{1}{2})$ and $\lambda' = N_r(m)$ we easily conclude the following.

Proposition 4.4 *The fixed point m_3 with $\frac{1}{2} < m_3 < \frac{3}{2}$ has eigenvalues λ, λ' with $0 < \lambda < 1$ and $\lambda' > 1$. Also*

$$\lambda \to 1, \quad \mu \to 1 \qquad as \qquad r \to 1 \quad (m_3 \to \tfrac{3}{2})$$

while

$$\lambda \to 0, \quad \mu \to \infty \qquad as \qquad r \to 0 \quad (m_3 \to \tfrac{1}{2}).$$

The eigendirection for μ is the m-axis. $\qquad\qquad\qquad\qquad\qquad\qquad\square$

Note that the eigendirection for λ would be the s-axis if there were no $O(3)$ terms in ϕ.

Since $(0, m_3)$ is a hyperbolic fixed point for h' it has a unique (local) smooth stable manifold W^s transverse to the m-axis. Then $\chi(W^s)$ is a smooth curve β through the origin in $\mathbf{R}^2$ and tangent to the s-axis from above ($\eta > 0$) or below ($\eta < 0$) according as $\sigma < 0$ or $\sigma > 0$, and the same holds in the original (σ, t) coordinates. By construction, since $h'(W^s) \subset W^s$ then $h(\beta) \subset \beta$ which in turn implies forward invariance of $\gamma := p(\beta) \cap \Pi_0^+$ under G. The dynamical properties of h' near the saddle point $(0, m_3)$ carry over via χ to the stated properties of G on and close to γ. This completes the proof of Theorem 4.1. $\qquad\qquad\qquad\qquad\qquad\qquad\square$

(b) The case $a'(\tau_*) < 0$

Here the horizon H for $(\tau, t) \neq (\tau_*, 0) = w_*$ locally lies in the region $v < 0$ and so $F : \Pi_0^+ \to V'$ and hence also $G : \Pi_0^+ \to \Pi_0^+$ are continuous maps in a neighbourhood of w_* in Π_0^+. Moreover, in a neighbourhood of the origin G is a homeomorphism onto its image and is differentiable away from w_*. In detail, with local coordinate $\tau = \tau_* + \sigma$ as before, we see that to first order F maps a neighbourhood $\mathcal{T}'$ of the origin in Π_0^+ onto a neighbourhood of the origin in the sector

$$\mathcal{T} : \quad 3\sigma + t \geq 0 \,, \, t \geq 0$$

in $\mathbf{R}^2$ (coordinates on V') which is then taken by ϕ to a neighbourhood of the origin in the region $\mathcal{T}''$ bounded by the positive σ-axis and an arc tangent to it given by

$$v = \tfrac{3}{8}a'(\tau_*)\sigma^2 + O(3)$$

in Π_0^-: see Figure 6. Finally, R maps $\mathcal{T}''$ to a similar if narrower region $R\mathcal{T}''$ in Π_0^+. From this geometry it is reasonable to suppose that under forward iteration of G all
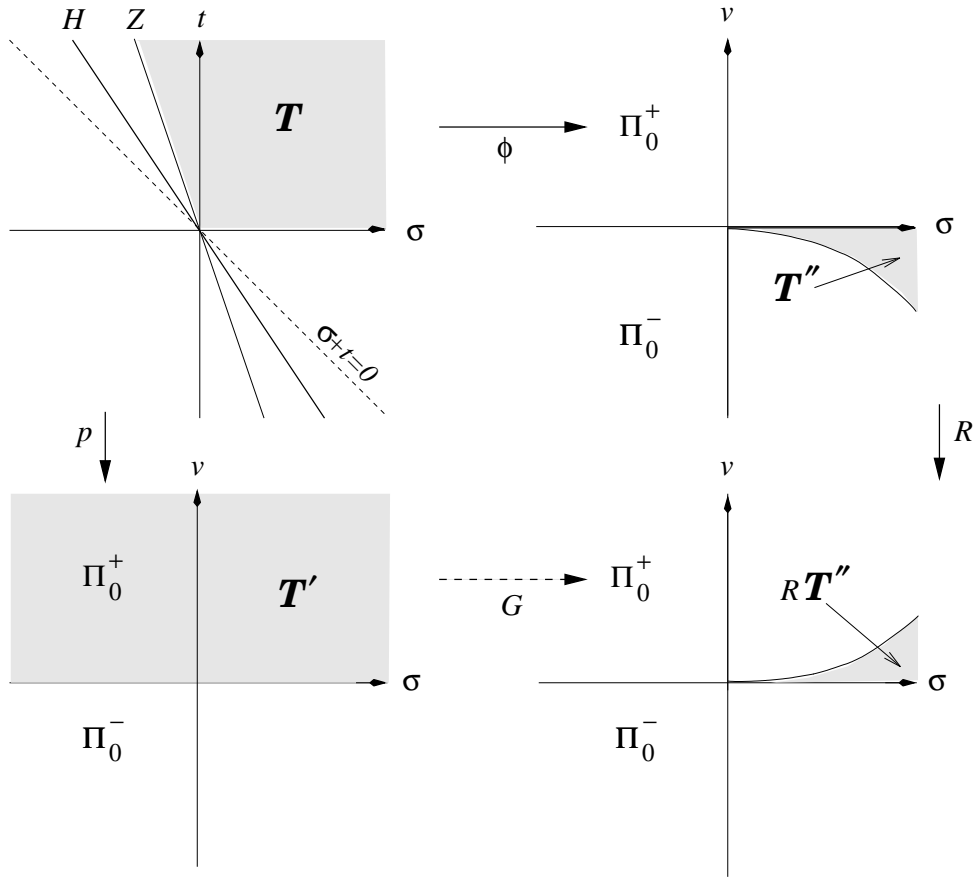
Figure 6. The actions of p, ϕ and R close to $(\tau_*, 0)$ with $a'(\tau_*) < 0$: here $\tau = \tau_* + \sigma$. The shaded area in the top left diagram represents the visible part of V', and the other shaded areas are its images under the relevant maps as indicated.

points of $\mathcal{T}'$ tend to the σ-axis Π_0. We now look more closely to verify that this is the case.

First consider an arc α_ℓ in V' given in (σ, t) coordinates by $t = \ell\sigma$ with $\ell \geq 0$ and $\sigma \geq 0$. From (18) and (19) we have

$$p(\sigma, \ell\sigma) = (\sigma, -k(3\ell + \ell^2)\sigma^2 + \ell\sigma^3\mu(\ell, \sigma)) \tag{32}$$

$$q(\sigma, \ell\sigma) = (\sigma(1 + \ell), -rk(3\ell + 2\ell^2)\sigma^2 + \ell\sigma^3\nu(\ell, \sigma)) \tag{33}$$

where μ, ν are continuous (in fact smooth) functions for (ℓ, σ) sufficiently small. The images of α_ℓ under p and q are locally the graphs of two smooth functions $v = \tilde{p}_\ell(\sigma)$ and $v = \tilde{q}_\ell(\sigma)$ for $\sigma \geq 0$. Given constants $K > 0, L > 0$ we can choose $\delta > 0$ such that

$$\tilde{p}_\ell(\sigma) > -k\ell(3 + \ell)(1 - K)\sigma^2$$

and

$$\tilde{q}_\ell(\sigma) < -rk\ell(3 + 2\ell)(1 + \ell)^{-2}(1 + L)\sigma^2$$

for $0 \leq \ell \leq \delta$ and $0 \leq \sigma \leq \delta$, where as before $k = \frac{1}{6}a'(\tau_*)$ and here $k < 0$. It then follows that

$$\frac{\tilde{q}_\ell(\sigma)}{\tilde{p}_{h\ell}(\sigma)} < \frac{3 + 2\ell}{(1 + \ell)^2(3 + h\ell)} \frac{1 + L}{1 - K} \frac{r}{h}$$

for any $0 < h < 1$. Choose K, L sufficiently small (and δ accordingly) so that $c := \frac{1+K}{1-L} r < 1$. Since $(3 + 2\ell) < (1 + \ell^2)(3 + h\ell)$ for all $\ell > 0$ and $h > 0$, the above estimates show that when $\ell, \sigma < \delta$ the arc $F \circ R \circ \phi(\alpha_\ell)$ lies below the arc $\alpha_{h\ell}$ in $\mathcal{T}$ when $c < h < 1$. In other words, when viewed in blown-up σ, ℓ coordinates in $\mathcal{T}$ the dynamics are dominated by exponential contraction in the ℓ-coordinate.

A similar argument applies to the derivatives $\tilde{p}'_\ell, \tilde{q}'_\ell$ of $\tilde{p}_\ell, \tilde{q}_\ell$ with respect to σ: for sufficiently small δ we can ensure that if $0 \leq \ell, \sigma \leq \delta$ then there exists $0 < h < 1$ such that $\tilde{q}'_\ell(\sigma) < \tilde{p}'_{h\ell}(\sigma)$ for $0 < \sigma < \delta$, and that therefore $\tilde{p}_\ell(\sigma)$ tends C^1-uniformly to zero for $0 \leq \sigma \leq \delta$. Thus we obtain the anticipated result:

Proposition 4.5 *Under iteration of G the images of the arc $p(\alpha_\ell)$ tend C^1-uniformly to the τ-axis over the interval $[0, \delta]$.* $\qquad\qquad\square$

Using this fact and the results from Section 3 we can give a complete description of the local dynamics around the tangency point w_*. Let D^+ denote the closed half-disk in $\mathbf{R}^2$ given by $D^+ = \{(x, y) \in \mathbf{R}^2 : x^2 + y^2 \leq 1, y \geq 0\}$, and let $E : D^+ \to D^+$ be the map described in polar coordinates $(x, y) = (\rho \cos \theta, \rho \sin \theta)$ by $\theta \mapsto \frac{1}{2}\theta$. The dynamics of E are a topological model for the dynamics of G close to w_*. More precisely:

Theorem 4.6 *There is a homeomorphism Ψ from D^+ onto a closed neighbourhood U of w_* in Π_0^+ with $\Psi(0, 0) = w_*$ and such that Ψ is a topological conjugacy between E and G, that is $\Psi \circ E = G \circ \Psi$. Moreover, Ψ can be chosen to be C^∞ off the x-axis. In particular, U is smoothly foliated (except perhaps on Π_0) by arcs of stable manifolds of points $w = (\tau, 0) \in \Pi_0$ with $\tau > \tau_*$, each arc having end-points on Π_0 on opposite sides of τ_*. See Figure 7.*

Proof. Choose positive numbers $0 < \delta_1 < \delta \in \mathbf{R}$ where δ is small enough to satisfy the conditions imposed in the proof of Proposition 4.5. By Theorem 3.2 there is a neighbourhood in Π_0^+ of the interval $J := [w_* + \delta_1, w_* + \delta] \subset \Pi_0$ that is smoothly foliated by stable manifolds of points of J. By Proposition 4.5 there is some positive integer n and interval $J' := [w'_1, w_*] \subset \Pi_0$ such that $G^n(J')$ is sufficiently C^1-close to J that it intersects the stable manifolds transversely. Let $G^n(w'_1) \in W^s(w_1)$, $w_1 \in \Pi_0$. It follows by backward iteration of G that the stable manifold of each $w \in J$ contains a closed arc with end-points on opposite sides of w_* in Π_0, and in particular $W^s(w_1)$ contains an arc from w'_1 to w_1. Since this construction applies for arbitrary δ_1 with $0 < \delta_1 \leq \delta$ we obtain a neighbourhood of w_* in Π_0^+ smoothly foliated (except perhaps on Π_0) by stable manifolds as claimed.

To construct a conjugacy Ψ we first construct a homeomorphism ψ from the sector $D(n)$ of D^+ given by $\frac{\pi}{2^{n+1}} \leq \theta \leq \frac{\pi}{2^n}$ to the region in Π_0^+ bounded by an arc of $G^{n+1}(J')$, and an arc of $G^n(J')$ together with an arc of $W^s(w_1)$. This can be done in such a way

that arcs in D^+ of constant distance from the origin are taken by ψ to arcs of stable manifolds of points in $[w_*, w_1]$. The homeomorphism ψ is then extended to Ψ on the whole of D^+ except for the positive x-axis by $\Psi(u) = G^{-\ell} \circ \psi \circ E^\ell(u)$ where ℓ is chosen to be the unique integer (positive or negative) such that $E^\ell(u) \in D(n)$. With care, ψ can be constructed at the boundary of $D(n)$ in such a way that Ψ is a diffeomorphism away from the origin. Finally, Ψ extends to the positive x-axis ($\theta = 0$) by continuity. $\square$
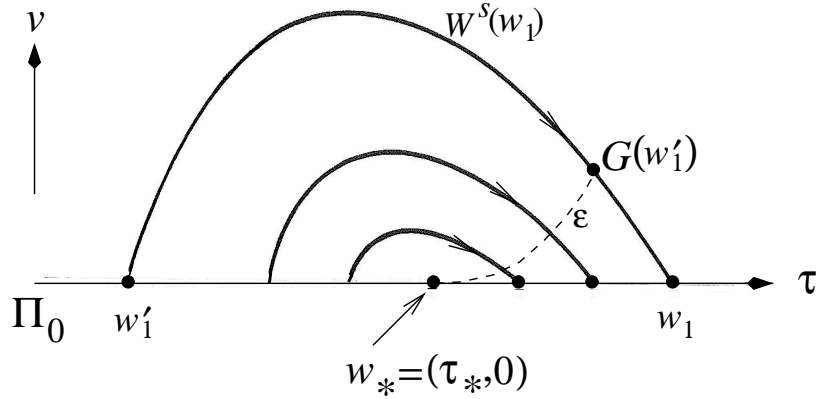
Figure 7. Chatter close to $w_* = (\tau_*, 0)$ with $a'(\tau_*) < 0$. Points of Π_0 with $\tau > \tau_*$ are limit points of nondegenerate chatter that becomes increasingly degenerate as $\tau \to \tau_*$ from above. The arc $[w_1', w_*]$ on Π_0 is taken by G to an arc ε tangent to Π_0 at w_*.

5. Further degeneracy: dynamics near a swan point

Finally we consider the dynamics of G close to a swan point $(\tau_*, 0)$; here $a(\tau_*) = a'(\tau_*) = 0$ but $a''(\tau_*) \neq 0$.

As before, we work with coordinates $\tau = \tau_* + \sigma$ and we write $(\sigma, \eta) = (s, sm) = \chi(s, m)$. Using (17) we see that the maps p and ϕ then become

$$p : (s, m) \mapsto (s, \ell s^3 (6m + 4m^2 + m^3 + O(s))) \tag{34}$$

$$\phi : (s, m) \mapsto (s(1 + m), -\ell s^3 (6m + 8m^2 + 3m^3 + O(s))) \tag{35}$$

where $\ell = -\frac{1}{2} 4 a''(\tau_*)$ and where the terms $O(s)$ denote smooth functions of (s, m) that vanish when $s = 0$.

In (s, m) coordinates the map h becomes $\bar{h} : (s, m) \mapsto (\bar{s}, \bar{m})$ where

$$s(1 + m) = \bar{s} \tag{36}$$

$$r s^3 (6m + 8m^2 + 3m^3 + O(s)) = \bar{s}^3 (6\bar{m} + 4\bar{m}^2 + \bar{m}^3 + O(s)) \tag{37}$$

and substituting the first equation into the second for $s \neq 0$ we obtain

$$r(6m + 8m^2 + 3m^3) = (1 + m)^3 (6\bar{m} + 4\bar{m}^2 + \bar{m}^3) + O(s).$$

The graphs of the two real-valued functions

$$f : m \mapsto r(6m + 8m^2 + 3m^3)(1 + m)^{-3} \tag{38}$$

$$g : m \mapsto 6m + 4m^2 + m^3 \tag{39}$$

intersect at a unique point m_* which lies in $(-1, 0)$. This proves the following.

Proposition 5.1 *The map $\bar{h}$ has a fixed point at $(0, m_*)$ and no other fixed point on the m-axis.*

It is easy to check from the graphs of f, g that $f'(m_*) > g'(m_*)$, and also to verify that

$$D\bar{h}(0, m_*) = \begin{pmatrix} 1 + m & 0 \\ * & f'(m_*)/g'(m_*) \end{pmatrix}. \tag{40}$$

This implies the next result.

Proposition 5.2 *The map $\bar{h}$ has a hyperbolic saddle fixed point at $(0, m_*)$. The m-axis is the unstable manifold, while the stable manifold is a smooth curve W^s through $(0, m_*)$ transverse to the m-axis.*

The interpretation of these results now depends on the sign of $a''(\tau_*)$.

If $a''(\tau_*) < 0$ then $a(\tau)$ has a local maximum at τ_* with $a(\tau_*) = 0$, and so from (5) we have $\frac{\partial}{\partial t} v_c(\tau, t) > 0$ for all (τ, t) in some neighbourhood of $w_* = (\tau_*, 0)$ in Π except at w_*. Therefore F is defined on a neighbourhood of w_* in Π and is a smooth local homeomorphism onto a neighbourhood of w_* in V'. Hence if $\beta = \chi(W^s)$ then $\gamma = p(\beta) \cap \Pi_0^+$ is a smooth forward invariant curve γ for G terminating at the swan point. As is clear from (34) this curve γ has cubic tangency with Π_0 at w_*.

Theorem 5.3 *Let $w_* = (\tau_*, 0) \in \Pi_0$ be a swan point with $a''(\tau_*) < 0$. There is a smooth arc $\gamma \subset \Pi_0^+$ with an end-point at w_*, cubically tangent to Π_0 at w_* from the side $\tau < \tau_*$ and otherwise lying in Π^+. The arc γ is forward invariant for G and locally unique in the sense of Theorem 4.1. The fixed point w_* is exponentially attracting for $G|\gamma$, and is weakly normally hyperbolic (repelling) for G. All points in a neighbourhood of w_* but not on γ lie on stable manifolds of regular points of Π_0 (nondegenerate chatter). See Figure 8.* □

Thus with $a''(\tau_*) < 0$ all initial data close to w_* lead to nondegenerate chatter, with the exception of those on the curve γ which exhibit a form of highly degenerate chatter.

If on the other hand $a''(\tau_*) > 0$ then we have $v_c(\tau, t) < 0$ for sufficiently small $t > 0$ and τ close to τ_*, and so the image under F of a neighbourhood of w_* in Π_0^+ will include no points close to w_*. Therefore the local analysis of low-velocity impacts which is the subject of this paper will not apply.

6. Unfolding the dynamics at the swan point

Typically (the precise conditions on the functions f and g in (1) are described in [16]) swan points will occur for only certain isolated values of c or of some other parameter
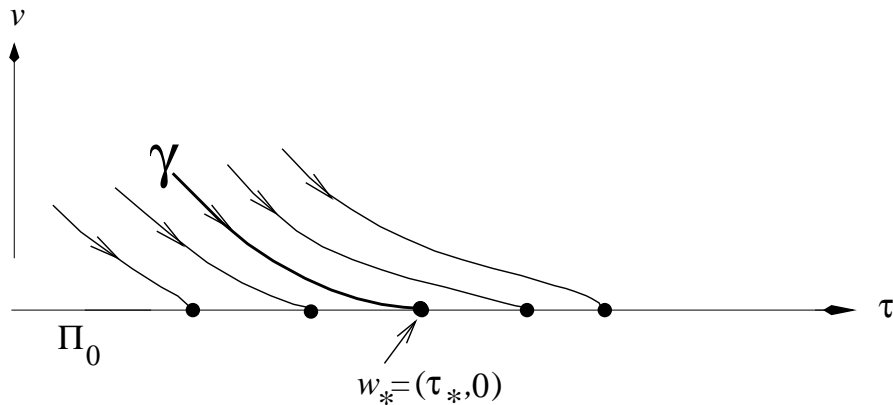
Figure 8. Stable manifolds of chatter points close to a swan point $(\tau_*, 0)$ where $a'(\tau_*) = 0$ and $a''(\tau_*) < 0$.

in the system: swan points are codimension-1 phenomena. Therefore it is important to consider the bifurcations in the local dynamics as a generic transition through a swan point takes place.

We shall take the parameter to be c for simplicity, although this is not crucial for the discussion. For clarity we also now re-introduce the c suffix in notation for the maps p_c, ϕ_c, F_c and G_c and the surface V_c'. We suppose that $a_c(\tau_*) = a_c'(\tau_*) = 0$ when $c = c_0$ and let

$$d(c, \tau) := a_c''(\tau) \frac{\partial a}{\partial c}(c, \tau)$$

where $a(c, \tau) = a_c(\tau)$. As c increases through c_0 the function $a_c(\tau)$ undergoes a Morse transition at which a pair of zeros τ_1, τ_2 of $a_c(\tau)$ is created or annihilated according to the sign of $d_0 := d(c_0, \tau_*)$. Note that under the Correspondence Principle the creation of two tangency points at a swan point corresponds to the creation of two cusps at a swallowtail (Figure 2(c)).

Without loss of generality we suppose $d_0 < 0$. As c increases through c_0 an interval (τ_1, τ_2) is created on which $a_c(\tau)$ reverses its sign, and a new component of P_c (a *swan* configuration) is created out of the point w_* as described in [16]. See Figure 9. The creation of the swan is in fact a version of the lips transition (Figure 2(a)) with particular geometry dictated by the context, a characteristic geometry of singular sets noted earlier by Bruce [11].

There are two cases to consider, according to whether $a_0''(\tau_*) := a_{c_0}''(\tau_*) > 0$ (*positive* swan point) or $a_0''(\tau_*) < 0$ (*negative* swan point).

6.1. Positive swan point: $a_0''(\tau_*) > 0$

For $c < c_0$ there are no low-velocity impacts occurring close to w_*, and for $c = c_0$ although the acceleration vanishes at τ_* there are still no low-velocity impacts. We
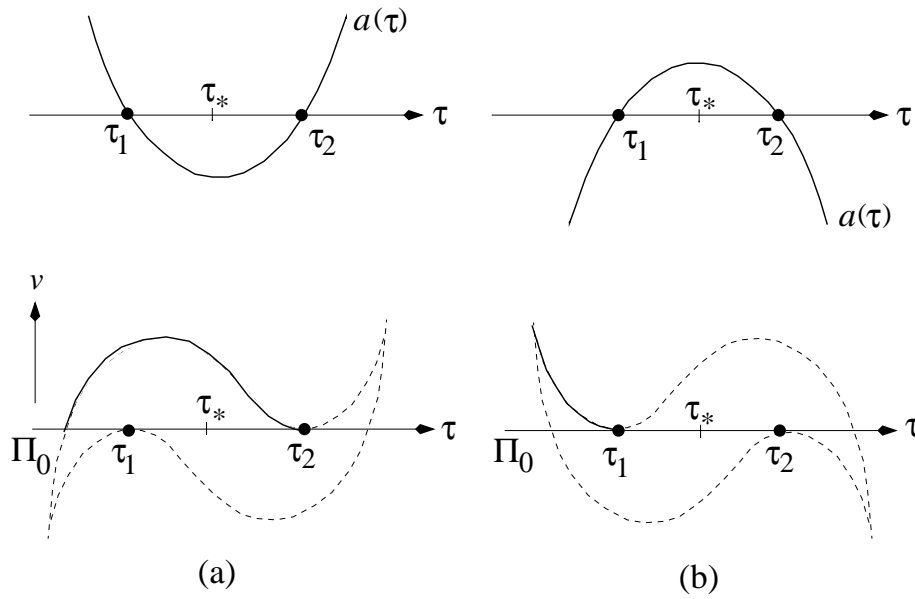
Figure 9. Graphs of $a(\tau)$ and associated swan configurations in the plane Π in two cases: (a) positive, (b) negative.
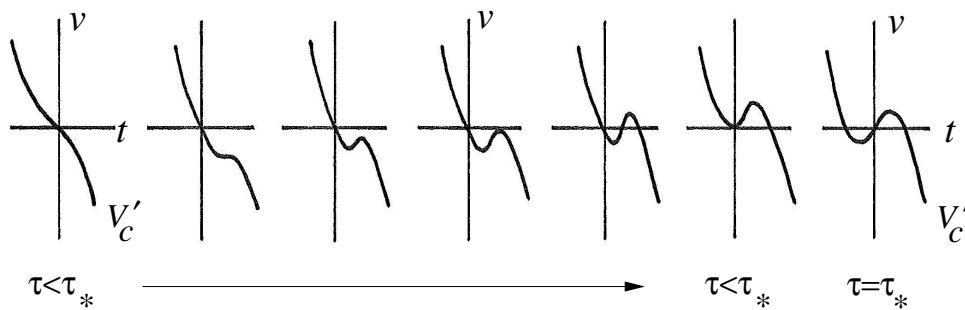

Figure 10. Sections through V'_c in the (t,v)-plane for increasing values of τ with $\tau \leq \tau_*$.

therefore focus on the low-velocity dynamical phenomena that are created when $c > c_0$. Once again we now suppose such c fixed sufficiently close to c_0 and dispense with it as a suffix.

To help picture the dynamics of G (and in particular the geometry of F) we show in Figure 10 a sequence of sections through $V' = V'_c$ at constant τ for various choices of $\tau \leq \tau_*$. This information can be obtained from the Taylor expansion (11), regarding
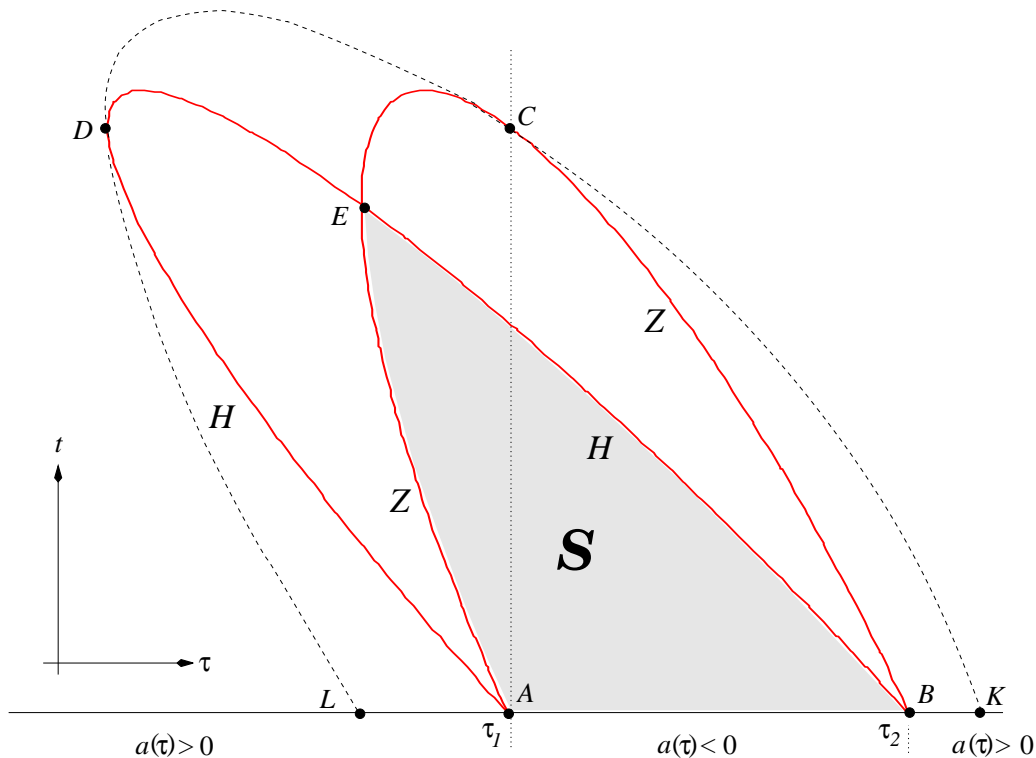
Figure 11. Positive swan configuration: the visible part $\mathcal{S}$ of V' is bounded by an arc of the horizon H and an arc of the zero locus Z as well as the interval AB of Π_0. See text for details.

$v_c(\tau_* + \sigma, t)$ as a function of t unfolded by the parameter σ. Analogous sketches for $\tau \geq \tau_*$ are obtained by reversing the signs of both t and v.

In Figure 11 we show the horizon H and the zero set Z in (τ, t)-coordinates on V', thus viewed from the 'vertical' v direction. Here $A = (\tau_1, 0)$ and $B = (\tau_2, 0)$ where $\tau_1 < \tau_2$ are the two zeros of $a(\tau)$ near τ_* for $c > c_0$ and close to c_0. The shaded area $\mathcal{S}$ indicates the connected component of the visible part of V' that contains the interval AB (see Section 2.2).

As already seen in Chapter 4, the dynamics of G close to A and B are as in Figure 5 and Figure 7 respectively. These combine to give the swan dynamics in the way that we now describe.

Figure 12(a) shows the same configuration as Figure 11 but viewed along the t-axis, or in other words its image in Π under the projection p. Points $p(C), p(D), \ldots$ are denoted $C', D', \ldots$; note that $A' = A$ and $B' = B$. The arc BE of H is taken by p to a smooth arc BE' in Π_0^+ tangent to Π_0 at B and transverse to Π_0 at E': together with the interval $E'B$ of Π_0 it bounds the simply-connected region $\mathcal{S}' = p(\mathcal{S}) \subset \Pi_0^+$.

Figure 12(b) shows the image of the configuration in Figure 11 under the re-set map ϕ, with points $\phi(C), \phi(D), \ldots$ denoted $C'', D'', \ldots$. The arc AE of Z is taken by ϕ to a smooth arc AE'' in Π_0^- tangent to Π_0 at A and transverse to Π_0 at E'' (part of the

apparent outline in view of the Correspondence Principle: see Proposition 2.3); together with the interval AE'' of Π_0 it bounds the simply-connected region $\mathcal{S}'' = \phi(\mathcal{S}) \subset \Pi_0^-$.

To construct the dynamics of G we compose the *inverse* of p with ϕ and then with the restitution R. The latter takes the arc AE'' in Π_0^- to a smooth arc in Π_0^+ tangent to Π_0 at A and transverse to Π_0 at E''. Its intersection with $\mathcal{S}'$ consists of a smooth arc ε' also tangent to Π_0 at A and with its other end-point N lying on the arc LB of the apparent outline. The arc ε' is the maximal extension (as far as the apparent outline LB) of the arc ε in Figure 7. The G-invariant curve γ at the degenerate chatter point B is tangent to Π_0 at B and transverse to Π_0 at its other point of intersection. It separates $\mathcal{S}'$ into two regions: one foliated by stable manifolds of points of AB (nondegenerate chatter), the other consisting of points that eventually leave $\mathcal{S}'$. See Figure 13.

### 6.2. Negative swan point: $a_0''(\tau_*) < 0$

For $c < c_0$ we have $a(\tau) < 0$ for all τ in a neighbourhood of τ_* and so Theorem 3.1 applies: every point lies in the stable manifold of some point of Π_0 and nondegenerate chatter takes place locally as in Figure 3(b).

For $c = c_0$ Theorem 5.3 applies: there is a smooth stable manifold for $(\tau_*, 0)$ that is cubically tangent to Π_0 and corresponds to highly degenerate chatter, while all other orbits experience nondegenerate chatter becoming increasingly degenerate as $\tau \to \tau_*$ from either side as in Figure 8. We therefore focus on the case $c > c_0$.

The analogue of Figure 10 for this case is obtained by inverting the v-axis. In Figure 14 we again show the horizon H and the zero set Z as viewed from the v-direction, with A, B as before corresponding to the values τ_1, τ_2 of τ where $a(\tau) = 0$. Now, however, it is a different region $\mathcal{T} = \mathcal{T}_1 \cup \mathcal{T}_2 \cup \mathcal{T}_3$ that is visible, bounded by the arc BC of Z, the arc DA of H, and the (dotted) arc DC which is the *shadow* of DA, that is the set of "next-hit" points starting from DA: more precisely it is the set of points $(\tau, v; t_1) \in V'$ for which there exists $t_0 > 0$ with $(\tau, v; t_0) \in DA$ but $(\tau, v; t) \notin V'$ for all $t_0 < t < t_1$. The visible part of V' is the region lying outside the loop $ADCBA$ (including AD but not including the open arc DC).

Under the correspondence principle in Figure 14 the points A, B each correspond to cusp points elsewhere on H: in fact B corresponds to D while A corresponds to its counterpart (not shown) with $t < 0$. Figure 15(a) shows the images $A', \ldots, E'$ of the points $A, \ldots, E$ of V' under projection p, while Figure 15(b) shows their images $A'', \ldots, E''$ under the re-set map ϕ. The only visible part of H is the arc from A to D: under p this projects to the arc AD' in Π_0^+ while under ϕ it is taken to the interval $A''D''$ on the τ-axis Π_0.

At points of the shadow arc CD apart from D the velocity $\dot{x}_c$ is nonzero (in fact it has to be negative) and so ϕ takes CD to an arc $C''D''$ with $v < 0$ except at D''; moreover C'' is a cusp point of P by Proposition 2.2. From this we see the nature of the discontinuity of the map $\phi \circ F$ (and hence of G): cutting Π^+ along the arc AD' then
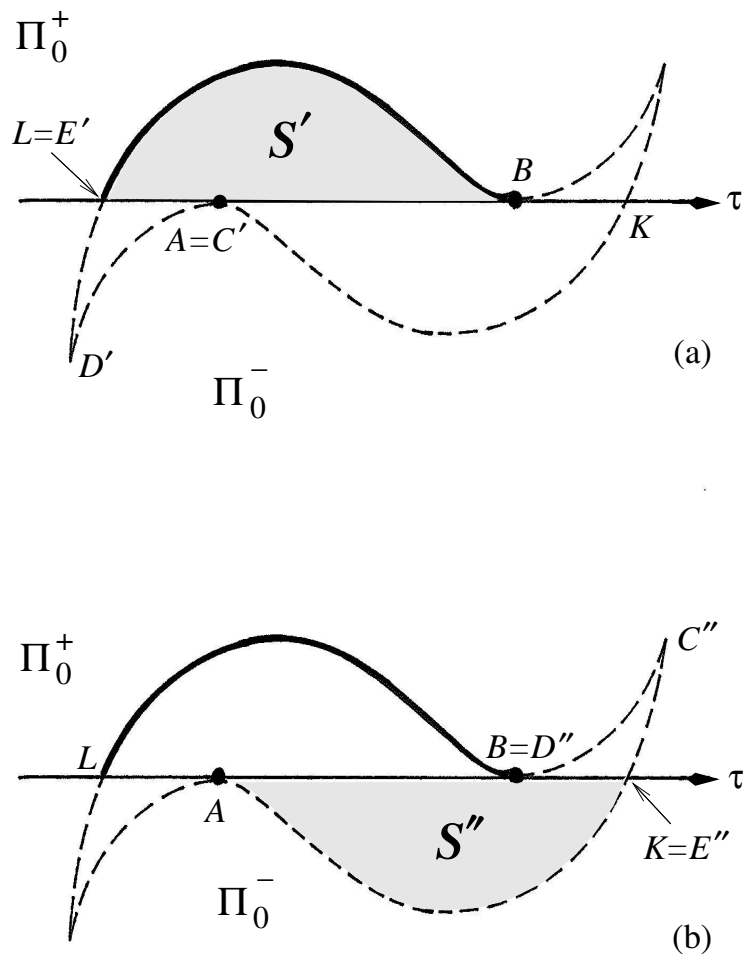
Figure 12. The images under (a) the projection p and (b) the re-set map ϕ of various regions of V' in Figure 11 for an unfolded positive swan point: see text for details.

mapping one edge (heavy) to the interval $A''D''$ of Π_0 and the other edge (dotted) to the arc $D''C''$. Meanwhile the interval AB of Figure 15(a) is mapped by F to the arc CB of Z which is then taken by ϕ to the arc $C''B$ of Figure 15(b).

These pictures repay contemplation in order to form a clear mental picture of the dynamics of G. Figure 16 shows schematically how $\phi \circ F$ takes each segment of the swan region into the next segment; remember, however, that the map G also incorporates the restitution R at each step and takes each of Π_0^+, Π_0^- into itself. We now describe the dynamics.

In Section 4.1 we have already obtained local models for the dynamics of G close to the two tangency points A and B (Figure 5 and Figure 7 respectively). As there are
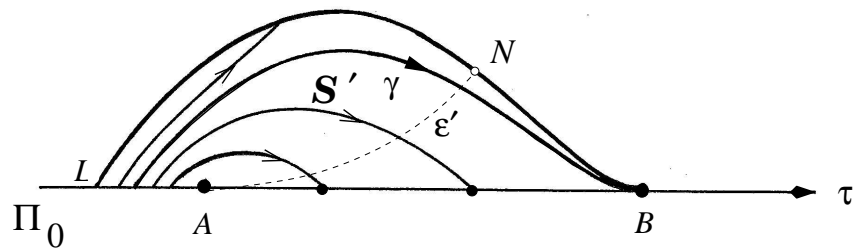
Figure 13. Invariant foliation for dynamics of G in the region S'. Outside S' the unfolding of the swan point gives no local information.
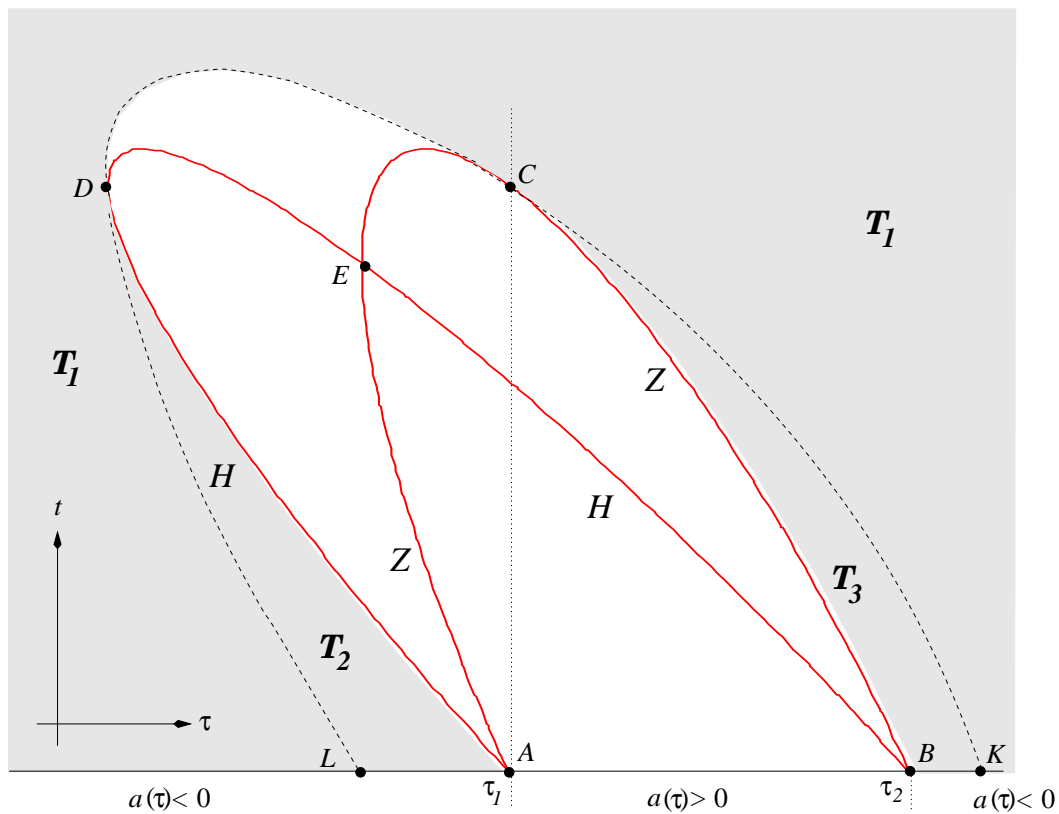
Figure 14. Negative swan configuration on V': the visible part (shaded) of V' here is bounded by an arc of H and an arc of Z together with an arc DC of the shadow of H.

no discontinuities of G close to B, the neighbourhood of B that is foliated by stable manifolds W^s_τ of points $(\tau, 0)$ with $\tau > \tau_2$ (by Theorem 4.6) must extend at least as far as the stable manifold $W^s_{\tau_3} = W^s(X)$ that contains the point A, where $X = (\tau_3, 0)$ with
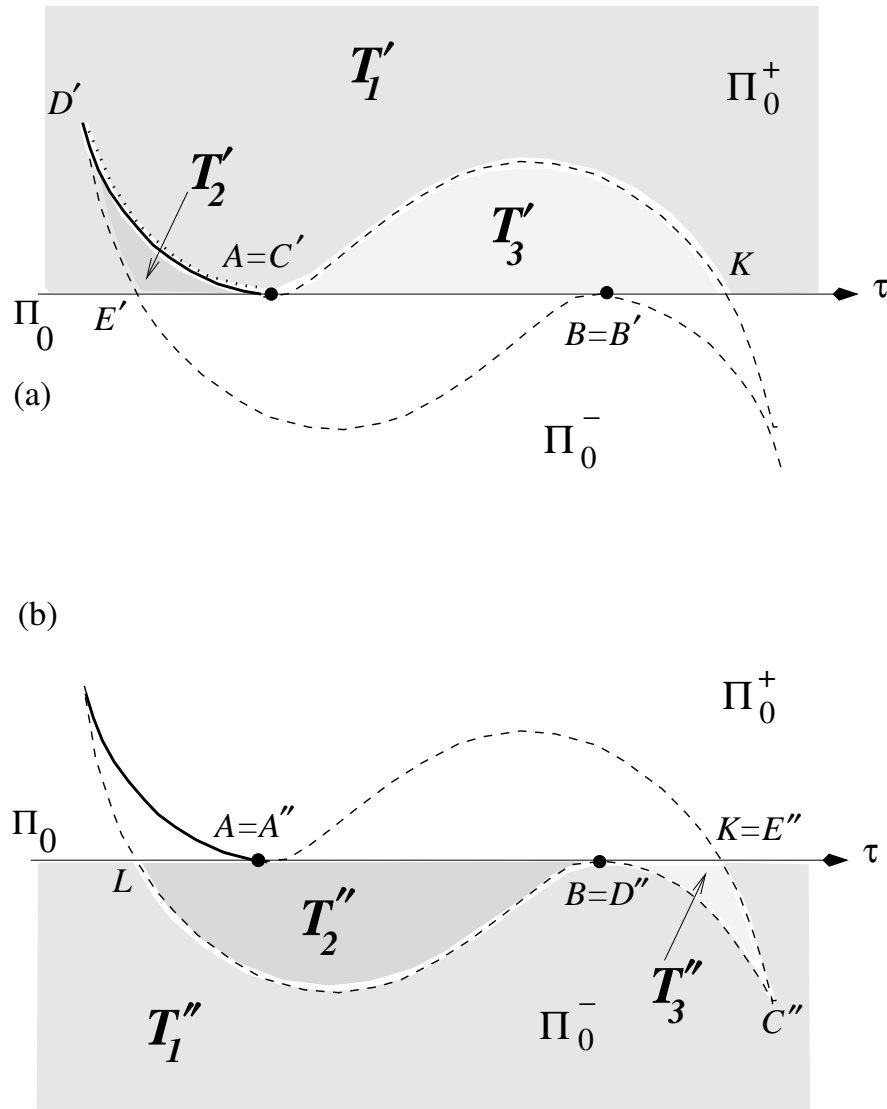
Figure 15. The images under (a) the projection p and (b) the re-set map ϕ of various regions of V' for an unfolded negative swan point: see text for details.

$\tau_3 > \tau_2$. See Figure 17.

Proposition 6.1 *The stable manifold $W^s(X)$ is tangent to Π_0 at A.*

Proof. We argue that $F(W^s(X)) \subset V'$ is tangent to Z at C, from which the result follows by applying p.

Since the map ϕ has a cusp singularity at C by Proposition 2.2, if $F(W^s(X))$ were not tangent to Z at C then $\phi \circ F(W^s(X))$ would be aligned with the direction of the cusp at C'' in Figure 15. In that case $R \circ \phi \circ F(W^s(X)) = G(W^s(X)) = W^s(X)$ would be tangent to the arc $\varepsilon'' = R(D''C'')$ at its endpoint $R(C'')$, and this is inconsistent with the geometry of chatter close to the point B where $a(\tau) = 0$ and $a'(\tau) < 0$ as in Figure 7: stable manifolds of points of Π_0 to the right of B are transverse to ε''. $\qquad\square$

Let λ denote the arc of $W^s(X)$ from A to $Q = W^s(X) \cap \varepsilon''$. The inverse image
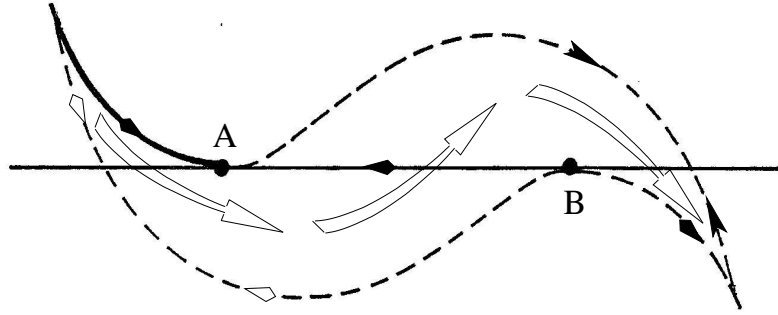
Figure 16. Schematic representation of the action of $\phi \circ F$ within the swan region. Matching arrows indicate arcs and their images. The third step is discontinuous along AB.

$G^{-1}(\lambda)$ is a closed loop around the discontinuity arc $\delta = AD'$ and with both ends at A. The inverse images of δ under iterates of G form a sequence of arcs tangent to Π_0 at the degenerate chatter point A and accumulating on its invariant arc γ, and therefore the inverse images of λ form a sequence of loops also accumulating on γ. Stable manifolds $W^s(Y)$ of points Y to the right of X on Π_0 (i.e. with $\tau > \tau_3$) and close to X oscillate more and more wildly under backwards iteration of G as they attempt to adhere to the loops of $G^{-n}(\lambda)$. Again see Figure 17.
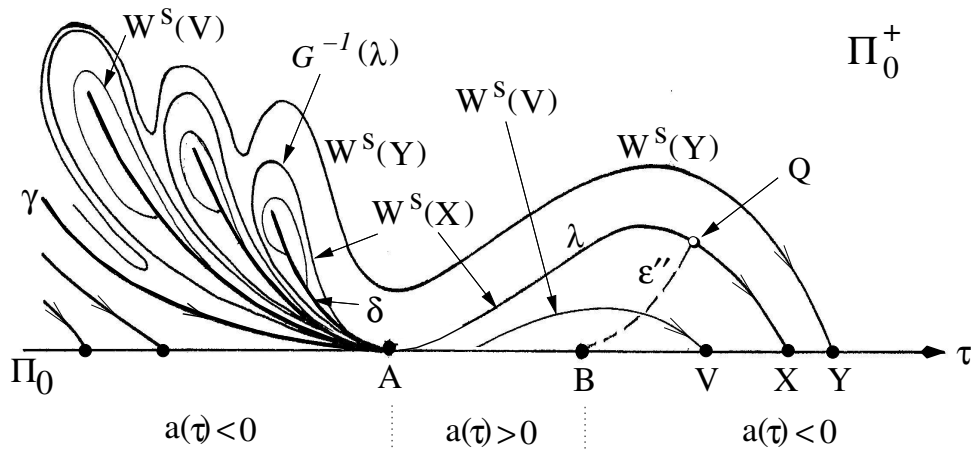
Figure 17. Dynamics of G created at unfolding of a negative swan point: see text for details.

7. Global dynamics

The dynamical phenomena that become apparent in the unfolding of a negative swan point give important clues about the global geometry for dynamics of an impact oscillator. In particular we see that the particular geometry of the smooth map $p \circ \phi^{-1}$ close to a tangency point $w_* = (\tau_*, 0) \in \Pi_0$ (so that $z = \phi^{-1}(w_*)$ is a cusp point of H) plays a key role. At a tangency point w_* where $a'(\tau_*) > 0$ the nearby stable manifolds W_τ^s with $\tau > \tau_*$ have infinitely many loops accumulating on the forward invariant curve γ that is the stable manifold of w_* Therefore we see that the global behaviour of the stable manifolds of degenerate chatter points, and in particular their intersections with unstable manifolds of fixed or periodic points elsewhere in the phase space Π_0^+, are crucial in organising the global effects of the complicated dynamics unleashed at a (negative) swan bifurcation. The swan configuration created at a negative swan point will persist until variation in the parameter c causes it to impinge on some other branch of the apparent outline P. Careful study of the generic ways in which this can happen will provide important tools for understanding the complicated global structure of discontinuous planar discrete dynamical systems modelling 1-degree of freedom impact oscillators.

References

[1] Alzate R, di Bernardo M, Montanaro U and Santini S 2007 Experimental and numerical verification of bifurcations and chaos in cam-follower impacting systems *J Nonlinear Dynamics* **50** 409–429 doi 101007/s11071-006-9188-8

[2] Andronov A A, Vitt A A and Khaikin S E 1959 *Theory of Oscillations*, Moscow; Eng. transl. Pergamon Press 1966

[3] Arnol'd V I 1986 *Catastrophe Theory, 2nd ed* (Berlin: Springer)

[4] Arnol'd V I, Gusein-Zade S M and Varchenko A N 1985 *Singularities of Differentiable Maps*,Vol I, (Boston, Mass.: Birkhäuser)

[5] Babitsky V I and Birkett N 1988 *Theory of Vibro-Impact Systems and Applications*, (Berlin Heidelberg: Springer-Verlag)

[6] di Bernardo M, Budd C J, Champneys A R, Kowalczyk P, Nordmark A B, Tost G O and Piiroinen P T 2008 Bifurcations in nonsmooth dynamical systems *SIAM Review* **50** 629–701

[7] di Bernardo M, Budd C J, Champneys A R and Kowalczyk P 2008 *Piecewise-Smooth Dynamical Systems: Theory and Applications* (London: Springer-Verlag)

[8] Brogliato B 1999 *Nonsmooth Mechanics* London: Springer-Verlag)

[9] Bruce J W 1984 Motion pictures: an application of singularity theory *J London Math Soc* **30** 160–170

[10] Bruce J W 1984 Seeing — the mathematical viewpoint *Math Intelligencer* **6** 18–25

[11] Bruce J W 1989 Geometry of singular sets *Math Proc Cambridge Philos Soc* **106** 495–509

[12] Bruce J W and Giblin P J 1984 *Curves and Singularities* (Cambridge: Cambridge University Press)

[13] Bruce J W and Giblin P J 1985 Outlines and their duals *Proc London Math Soc* **50** 552–570

[14] Budd C J and Dux F J 1994 Chattering and related behaviour in impact oscillators *Phil Trans R Soc London A* **347** 365–389

[15] Budd C J, Dux F J and Cliffe A 1995 The effect of frequency and clearance variations on single-degree-of-freedom impact oscillators *J Sound and Vibration* **184** 475–502

[16] Chillingworth D R J 2002 Discontinuity geometry for an impact oscillator *Dynamical Systems* **17** 389–420

[17] Chin W, Ott E, Nusse H E and Grebogi C 1994 Grazing bifurcation in impact oscillators *Phys Rev E* **50** 4427–4444

[18] Dankowicz H and Jerrelind J 2005 Control of near-grazing dynamics in impact oscillators *Proc Roy Soc London A* **461:2063** 3365–3380

[19] Demeio L and Lenci S 2006 Asymptotic analysis of chattering oscillations for an impacting inverted pendulum *Quarterly J Mech Appl Math* **59** 419–434

[20] Fidlin A 2006 *Nonlinear Oscillations in Mechanical Engineering* (Berlin Heidelberg: Springer-Verlag)

[21] Foale S and Bishop S R 1992 Dynamical complexities of forced impacting systems *Phil Trans R Soc London A* **338** 547–556

[22] Golubitsky M and Guillemin V 1973 *Stable Mappings and their Singularities* (New York: Springer-Verlag)

[23] Guckenheimer J and Holmes P 1983 *Nonlinear Oscillations Dynamical Systems and Bifurcations of Vector Fields* (New York: Springer) (revised ed. 2002)

[24] Hayashi C 1985 *Nonlinear Oscillations in Physical Systems* (Princeton: Princeton University Press)

[25] Hindmarsh M and Jeffries D 1984 On the motion of the offset impact oscillator *J Physics A: Math Gen* **17** 1791–1803

[26] Hirsch M W, Pugh C C and Shub M 1977 *Invariant Manifolds* Lect Notes in Math **583** Springer-Verlag

[27] Hasselblatt B and Pesin Ya 2005 Partially hyperbolic dynamical systems in *Handbook of Dynamical Systems* IB Elsevier

[28] Lamba H 1995 Chaotic regular and unbounded behaviour in the elastic impact oscillator *Physica D* **82** 117–135

[29] Ivanov A P 1994 Impact oscillations: linear theory of stability and bifurcations *J Sound and Vibration* **178** 361–378

[30] Kleczka M, Kreuzer E and Schiehlen W 1992 Local and global stability of a piecewise linear oscillator *Phil Trans R Soc London A* **338** 533–546

[31] Mason J F, Homer M E and Wilson R E 2007 Mathematical models of gear rattle in Roots blower vacuum pumps *J Sound and Vibration* **308** 431–440

[32] Molenaar J, de Weger J G and van de Water W 2001 Mappings of grazing-impact oscillators *Nonlinearity* **14** 301–321

[33] Nordmark A B 1991 Non-periodic motion caused by grazing incidence in an impact oscillator *J Sound and Vibration* **145** 279–297

[34] Nordmark A B 1997 Universal limit mapping in grazing bifurcations *Phys Rev E* **55** 266–270

[35] Pavlovskaia E and Wiercigroch M 2003 Modelling of vibro-impact system driven by beat frequency *Int J Mech Sci* **45** 623–641

[36] Peterka F and Vacík J 1992 Transition to chaotic motion in mechanical systems with impacts *J Sound and Vibration* **154** 95–115

[37] Schmidt G and Tondl A 1987 *Non-Linear Vibrations* (Cambridge: Cambridge University Press)

[38] Shaw S W and Holmes P J 1983 A periodically forced piecewise linear oscillator *J Sound and Vibration* **90** 129–155

[39] Sotomayor J and Teixeira M A 1988 Vector fields near the boundary of a 3-manifold pp 169–195 in *Lecture Notes in Mathematics* v. 1331 Springer

[40] Stewart D 2000 Rigid-body dynamics with friction and impact *SIAM Review* **42** 3–39

[41] Stone E and Askari A 2002 Nonlinear models of chatter in drilling processes *Dynamical Systems* **17** 65–85

[42] Szalai R and Osinga H M 2008 Unstable manifolds of a limit cycle near grazing *Nonlinearity* **21** 273–284

[43] Takens F 1971 Partially hyperbolic fixed points *Topology* **10** 133–147

[44] Thompson J M T and Ghaffari R 1982 Chaos after period doubling bifurcations in the resonance of an impact oscillator *Phys Lett* **91A** 5–8

[45] Valente A X C N, McClamroch N H and Mesić I 2003 Hybrid dynamics of two coupled oscillators that can impact a fixed stop *Int J Non-Linear Mech* **38** 677-689

[46] Virgin L N and Begley C J 1999 Grazing bifurcations and basins of attraction in an impact-friction oscillator *Physica D* **130** 43–57

[47] Wagg D J and Bishop S R 2001 Chatter sticking and chaotic impacting motion in a two-degree of freedom impact oscillator *Int J Bifurcation and Chaos* **11** 57–71

[48] Wagg D J and Bishop S R 2004 Dynamics of a two degree of freedom vibro-impact system with multiple motion limiting constraints *Int J Bifurcation and Chaos* **14** 119–140

[49] Whiston G W 1987 The vibro-impact response of a harmonically excited and preloaded one-dimensional linear oscillator *J Sound and Vibration* **115** 303–319

[50] Whiston G W 1987 Global dynamics of a vibro-impacting linear oscillator *J Sound and Vibration* **118** 395–429

[51] Whiston G W Singularities in vibro-impact dynamics 1992 *J Sound and Vibration* **152** 427–460

[52] Whitney H On singularities of mappings of Euclidean spaces I 1955 Mappings of the plane into the plane *Ann Math* **62** 374–410

[53] Zhao X and Dankowicz H 2006 Unfolding degenerate grazing dynamics in impact actuators *Nonlinearity* **19** (2006) 399–418